



The Catastrophe Optics of Liquid Drop Lenses

Author(s): J. F. Nye

Source: *Proceedings of the Royal Society of London. Series A, Mathematical and Physical Sciences*, Vol. 403, No. 1824 (Jan. 8, 1986), pp. 1-26

Published by: Royal Society

Stable URL: <http://www.jstor.org/stable/2397899>

Accessed: 27-11-2017 01:50 UTC

JSTOR is a not-for-profit service that helps scholars, researchers, and students discover, use, and build upon a wide range of content in a trusted digital archive. We use information technology and tools to increase productivity and facilitate new forms of scholarship. For more information about JSTOR, please contact support@jstor.org.

Your use of the JSTOR archive indicates your acceptance of the Terms & Conditions of Use, available at <http://about.jstor.org/terms>



Royal Society is collaborating with JSTOR to digitize, preserve and extend access to *Proceedings of the Royal Society of London. Series A, Mathematical and Physical Sciences*

JSTOR

The catastrophe optics of liquid drop lenses

BY J. F. NYE, F.R.S.

*H. H. Wills Physics Laboratory, University of Bristol,
Tyndall Avenue, Bristol BS8 1TL, U.K.*

(Received 29 May 1985)

[Plates 1–11]

The optical caustics associated with a number of higher umbilic catastrophes have been studied experimentally by passing light through drops of water resting on a horizontal glass slide. When the perimeters of the drops were constrained to have the symmetry of a square (4mm), the caustics were organized by X_9 , which is the lowest catastrophe of corank 2 to possess a modulus. Changing the shape of the perimeter of a thin drop of this symmetry that is large enough to be affected by gravity has the effect of sweeping the modulus K through its complete range -6 to $+2$; in particular, one can study the physical caustics as K passes through the special value -2 , which is mathematically excluded from X_9 . Similar variations of K are produced by varying the size of thin drops with square outlines, or simply by adding water to a drop of fixed outline so that its profile becomes highly curved. Twofold (2mm) and fourfold (4mm) symmetries are the only ones that allow X_9 , with its full range of moduli, to participate. However, the range of caustics produced by drops with these symmetries cannot be understood in terms of X_9 alone; to explain the observed details it is necessary to take account of the fact that X_9 is embedded in the higher catastrophe $Y_{2,2}^1$.

A theory of the drop profile under the combined effects of surface tension and gravity, valid for small slopes, leads to a calculation of the caustics in the paraxial approximation. This is completely adequate to explain the observations, for thin drops, but, as a surprising example of structural stability, it also suffices when the drops are highly curved and the paraxial approximation breaks down. However, the paraxial theory does fail, as expected, when highly curved drops are inverted so that they hang from the lower surface of the glass slide. Then the X_9 patterns due to gravity are opposed to those due to non-paraxiality; for a drop of square outline, filled nearly to the point where it is about to detach itself, and illuminated from below, the two effects exactly cancel when the side is 7.3 mm. Analysis of these patterns of fourfold symmetry helps in understanding the caustic patterns produced by drops having other symmetries, or no symmetry at all.

1. INTRODUCTION

A drop of water placed on a horizontal glass slide behaves, with its natural irregularities, as an imperfect lens. For example, when it is illuminated by a parallel beam of light it produces a three-dimensional system of caustics, which may be

examined in detail under a microscope. The theoretical study of the caustics – they are highly organized in spite of the irregularity of the drop – is based on catastrophe theory.

Catastrophe optics (Berry 1976; Berry & Upstill 1980) has been applied specifically (Nye 1978) to the comparatively simple case where the glass substrate is horizontal, where the slope of the drop surface is everywhere small (so that the drop is thin, in the sense of thin lens theory) and where the drop is small enough in size for the effect of gravity, in creating a non-uniform pressure, to be neglected. Experimentally, the perimeter of a drop can be controlled by allowing the water to span a small hole of chosen shape, cut in opaque tape, which is stuck to a microscope slide. With this technique for fixing its edge, the shape of the drop can be varied by tilting the slide, so that gravity now has an appreciable effect. In spite of the distortion by gravity the drop may still be ‘thin’, and in this régime catastrophes of higher codimension (D_5 and E_6) have been studied (Nye 1979).

During these experiments it was noticed that, if the hole in the tape, which was typically about 3 mm across, was sufficiently charged with water to make the slopes of the drop large, the caustic patterns changed in a striking way. The ‘focus’ was now much nearer to the drop and much brighter, as one would expect, but its caustic structure had many new features that were only resolvable under high magnification. Alternatively, if the hole in the tape was large enough for gravity to have an appreciable effect on the drop profile, similar new caustic structure appeared.

To subdue some of the complication that exists in the pattern from a completely irregular drop, it was decided to impose some symmetry, and, for a reason that will now be explained, fourfold symmetry (two-dimensional point group 4mm) was chosen for detailed study. Specifically, water drops were formed in square holes with the glass substrate horizontal. In some experiments the size of the hole (up to 15 mm on a side) was sufficiently large for gravity to affect the comparatively flat profile, while in others the hole was smaller and the drop much more highly curved.

The caustic patterns formed by drops having this symmetry are organized, in part, by the catastrophe X_9 . This is of higher codimension (dimension of control space), namely 8, than the catastrophes previously studied by the drop method, and is of special interest because it is the lowest (of corank 2) to possess modality. This means that its germ is expressible not as a single polynomial but as a one-parameter family of polynomials, the different members being specified by a modulus K . The relevant germ of X_9 is (Callahan 1982a)

$$x^4 + Kx^2y^2 + y^4 \quad (x, y \text{ real}),$$

and it splits into two sub-families according to the range of K :

$${}^0X_9: K > -2, \quad K \neq 2;$$

$${}^4X_9: K < -2.$$

The cases $K = \pm 2$ are excluded because they give singularities $(x^2 \pm y^2)^2$ of infinite codimension.

Now it became apparent that the effect of adding more water to a drop in a square hole, or, more generally, in a hole of the same symmetry, so making the drop more bulbous, was steadily to increase K from the value -6 , appropriate (as we shall see) to a very thin drop, through the excluded value $K = -2$, to approach $K = 2$, which would be appropriate for a drop of perfect circular symmetry. Thus holes of this symmetry (4mm) gave the opportunity of examining the experimental implications of varying a modulus. It was of particular interest to see how the caustics would evolve through the value $K = -2$.

The effects of other imposed symmetries, 2, 3, 5, 6-fold and so on, and indeed the effects of no symmetry at all, are more easily understood in the light of the results for the 4-fold case, and some remarks are made on this at the end of the paper.

Theoretical and numerical studies (Callahan 1982*a,b*; Upstill 1979) have concentrated on describing some of the main features of the unfolding of X_9 . The present study, by contrast, is experimentally based, like that of Upstill *et al.* (1982) and Hajnal *et al.* (1984). Rather than studying the unfolding of X_9 *per se*, it seeks to understand, and to put into context within catastrophe theory, the caustics produced by water drops of controlled perimeter. In this physical system X_9 is found embedded in still higher singularities, which play an essential part, as we shall see, in determining the observed caustics. This will be a main theme of the paper.

2. THE SHAPE OF THE DROP

With origin O at the summit of the drop (figure 1*a*), take axes $O\bar{x}, O\bar{y}$ in the horizontal tangent plane, with $O\bar{z}$ vertical, and specify the shape of the drop by the distance $\bar{h}(\bar{x}, \bar{y})$ of its upper surface below the plane $\bar{z} = 0$. We consider first the case where the surface slope is everywhere small, $|\text{grad } \bar{h}| \ll 1$. Then the shape of the drop is governed by surface tension according to the equation

$$\frac{\partial^2 \bar{h}}{\partial \bar{x}^2} + \frac{\partial^2 \bar{h}}{\partial \bar{y}^2} = \frac{\bar{p}_0}{T} + \frac{\rho g}{T} \bar{h}. \quad (1)$$

Here \bar{p}_0 is the excess pressure in the water at O, T is the surface tension, ρ is the density and g is the acceleration of gravity. Note the inclusion of the last term, which represents the linear variation of pressure with height.

If a plane wave is now incident normally on the lower, flat, surface of the drop, Snell's law implies that the wavefront emerging from the upper surface, specified by its height $\bar{f}(\bar{x}, \bar{y})$ above $\bar{z} = 0$, is (in the approximation of small slopes) a scaled mirror image of $\bar{h}(\bar{x}, \bar{y})$, thus:

$$\bar{f}(\bar{x}, \bar{y}) = (n - 1) \bar{h}(\bar{x}, \bar{y}), \quad (2)$$

n being the refractive index. Then

$$\frac{\partial^2 \bar{f}}{\partial \bar{x}^2} + \frac{\partial^2 \bar{f}}{\partial \bar{y}^2} = \frac{1}{R_0} + \frac{\bar{f}}{l_0^2}, \quad (3)$$

where $R_0^{-1} = (n - 1)\bar{p}_0/T$ is the total curvature of the wavefront at O (so that its radius of curvature, when it has 4-fold symmetry, is $2R_0$). We have introduced the length $l_0 = (T/\rho g)^{\frac{1}{2}}$ that is characteristic of surface tension problems with gravity.

We now specify a scale length l . This could be the width of the aperture, or l_0 , but we keep it general for the moment. Later we shall put $l = l_0$, but we wish to be able to approach the limit $l_0 \rightarrow \infty$ (no effect of gravity) without l changing. So define dimensionless variables x, y, f by

$$\bar{x} = lx, \quad \bar{y} = ly, \quad R_0 \bar{f} = l^2 f, \quad (4)$$

giving for equation (3),

$$\frac{\partial^2 f}{\partial x^2} + \frac{\partial^2 f}{\partial y^2} = 1 + \left(\frac{l}{l_0}\right)^2 f. \quad (5)$$

We now impose the symmetry (4mm) of a square, with sides parallel to Ox and Oy, but this does not, of course, restrict the perimeter to be a square. In the absence of gravity ($l_0 \rightarrow \infty$) the last term disappears. In this case the general solution, subject to $f = 0$ and $\partial f / \partial x = \partial f / \partial y = 0$ at the origin, is

$$f = \frac{1}{4}(x^2 + y^2) + a_4(x^4 - 6x^2y^2 + y^4) + O(8) \quad (l_0 \rightarrow \infty) \quad (6)$$

or, in polar coordinates r, θ ,

$$f = \frac{1}{4}r^2 + a_4 r^4 \cos 4\theta + a_8 r^8 \cos 8\theta + \dots \quad (l_0 \rightarrow \infty). \quad (7)$$

The coefficients $a_4, a_8 \dots$ are determined by the shape of the aperture (its size being accommodated by the scale length l).

If, on the other hand, gravity is always present, l_0 is not infinite and we may choose it as our scale length: $l = l_0$. The right-hand side of (5) is now $1 + f$ and the appropriate general solution is

$$f = -1 + I_0(r) + c_4 I_4(r) \cos 4\theta + c_8 I_8(r) \cos 8\theta + \dots \quad (l = l_0), \quad (8)$$

where the $I_n(r)$ are modified Bessel functions. Replacing the $I_n(r)$ by their power series we have

$$f = \frac{1}{4}r^2 + \left(\frac{1}{64} + \frac{c_4}{2^4 \times 4!} \cos 4\theta\right)r^4 + \left(\frac{1}{4^3 \times 36} + \frac{c_4}{2^6 \times 5!} \cos 4\theta\right)r^6 + O(8) \quad (l = l_0). \quad (9)$$

Thus, up to $O(6)$ there is only one adjustable parameter, namely c_4 . A second enters in $O(8)$, namely c_8 . Notice that this solution differs from that for no gravity (equation (7)) in containing terms in r^6 .

We now keep the scale length l general, so that we can deal equally well with zero or non-zero gravity. The appropriate general solution of (5) in cartesian coordinates is found by substituting a general power series for x, y , thus:

$$\begin{aligned} f = & \frac{1}{4}(x^2 + y^2) + C(x^4 + Kx^2y^2 + y^4) \\ & + C\left(\frac{l}{l_0}\right)^2 \left(\frac{12-K}{360}x^6 + \frac{K}{24}x^4y^2 + \frac{K}{24}x^2y^4 + \frac{12-K}{360}y^6\right) + O(8). \end{aligned} \quad (10)$$

The constant C has to be non-zero if we are to have any anisotropy contributed by the fourth-order terms, and K is a constant (later to be identified with the modulus K of X_9) that is related to C by

$$K = \frac{1}{8C} \left(\frac{l}{l_0} \right)^2 - 6. \quad (11)$$

As $l_0 \rightarrow \infty$, we see that $K \rightarrow -6$ (since $C \neq 0$) and that the sixth-order term in (10) disappears, both results being in accordance with (6).

Comparison of solution (10), for $l = l_0$, with solution (8) shows that the coefficient c_4 is related to K by

$$c_4 = 6(2 - K)/(K + 6) \quad (l = l_0). \quad (12)$$

This is important for our purpose because it shows that the range of positive c_4 corresponds to the range $-6 < K < 2$, while the rest of the range of K corresponds to negative c_4 . But the sign of c_4 in (8) may be changed merely by altering the datum azimuth for θ by $\frac{1}{4}\pi$. Thus, for any given drop shape, K may always be brought within the range $-6 < K < 2$ by appropriate choice of coordinates.

The significant point is that as c_4 , which decides the amplitude of the $\cos 4\theta$ term in (8), decreases from infinity to zero, so the value of K increases from -6 , the zero-gravity value, to 2 , the value that makes the fourth-order terms isotropic. Figure 2, which is based on observation, shows a semi-quantitative way how the value of K , for thin drops, depends on the shape and size of the aperture. The abscissa is a rough measure of ‘squareness’ or ‘roundness’. Changing from a square on the left to a circle on the right with a fixed width of, say, 3 mm, changes K from a value near -6 to 2 .

To understand the effect of size on the drop profile consider first a circular hole. It is easy to show that the difference of pressure, due to gravity, between the top and bottom of the drop is small compared with the average excess pressure if the hole diameter is much less than $4l_0$. Within the régime of small slopes this condition, remarkably enough, is independent of the thickness of the drop. (When the drop is very thin the pressure difference is very small, but so is the pressure excess.) By extending this result to square holes we can infer that for a thin drop in a small square hole, gravity is not important and essentially $K = -6$. But, for a large square hole, gravity is always important, however thin the drop, and so K will depart from -6 . In practice, as figure 2 shows, one cannot achieve the whole range of K from -6 to $+2$ by using thin drops in square holes; the range $0 < K < 2$ requires some rounding of the aperture. It is also clear from figure 2 that a small, thin, circular drop has indeterminate K ; this explains why drops approximating these conditions can give confusing caustic patterns.

All this is for small slopes. A theory for large slopes would be more involved, because not only would the expression for drop curvature be nonlinear in \bar{h} , but we could no longer use a linearized form for Snell’s law. However, it was observed that, when a drop was formed in a small square hole (say, of side 1.4 mm = $0.52l_0$) and gradually loaded droplet by droplet with more water until its surface was so highly curved as to be nearly vertical at the edges, the sequence of caustics was exactly the same as that obtained by varying the shape and size of thin drops;

the only difference was that now all values of K between -6 and nearly $+2$ could be obtained with a single hole. The increase of K in such a small drop must be due to the large slopes and high curvatures, in contrast to the larger thin drops, where we see the effect of gravity in producing a non-uniform pressure. This is a remarkable example of structural stability in a system of caustics: the essential features of the caustics from a drop of large slopes and high curvatures, which would be very hard to calculate analytically, are the same as those arising from the effect of gravity on a drop of small slopes, which we calculate here by simple methods.

The experimental technique was, in fact, to use a square hole of size $4.6 \text{ mm} = 1.7 l_0$, increasing the amount of water in it until eventually symmetry was broken by the drop transgressing one of its boundaries. In this way the sequence of caustics shown in figure 7 (to be discussed in detail later) was established. Then other shapes and sizes of holes were used, but keeping the drops thin, to verify that the essential features of the caustics (in particular the crucial lips and umbilic loci) were the same.

3. THE GENERATING FUNCTION

The next step is to relate the shape of the initial wavefront to the caustics. We denote a general point in the image space where the caustics are formed by coordinates (X, Y, Z) and, as in Nye (1979), define a distance function, or generating function, by

$$\bar{\phi}(\bar{x}, \bar{y}; X, Y, Z) = \bar{f}(\bar{x}, \bar{y}) - \frac{\bar{x}^2 + \bar{y}^2}{2Z} + \frac{\bar{x}X + \bar{y}Y}{Z}. \quad (13)$$

This is related to the distance between the general observation point (X, Y, Z) and the general wavefront point $(\bar{x}, \bar{y}, \bar{f})$. It is chosen to have the property that, for fixed X, Y, Z the condition for it to be stationary with respect to \bar{x}, \bar{y} , namely

$$\partial \bar{\phi} / \partial \bar{x} = \partial \bar{\phi} / \partial \bar{y} = 0,$$

gives

$$\frac{\partial \bar{f}}{\partial \bar{x}} = \frac{\bar{x} - X}{Z}, \quad \frac{\partial \bar{f}}{\partial \bar{y}} = \frac{\bar{y} - Y}{Z}. \quad (14)$$

These are the conditions, within the approximation $Z \gg \bar{f}$, that the line joining (X, Y, Z) to $(\bar{x}, \bar{y}, \bar{f})$ is normal to the wavefront: in other words, that it represents a ray. Thus the stationary condition on $\bar{\phi}$ generates the ray through (X, Y, Z) .

To obtain a suitable non-dimensional form introduce a non-dimensional generating function ϕ and non-dimensional control variables W_1, W_2, W_3 , thus:

$$\left. \begin{aligned} \phi &= \frac{R_0}{Cl^2} \bar{\phi}, \\ W_1 &= \frac{R_0}{Cl} \frac{X}{Z}, \quad W_2 = \frac{R_0}{Cl} \frac{Y}{Z}, \quad W_3 = \frac{Z - 2R_0}{4CZ}. \end{aligned} \right\} \quad (15)$$

The new horizontal controls W_1 and W_2 measure angles X/Z and Y/Z , while the vertical control W_3 is a measure of distance above the focus at height $2R_0$. With

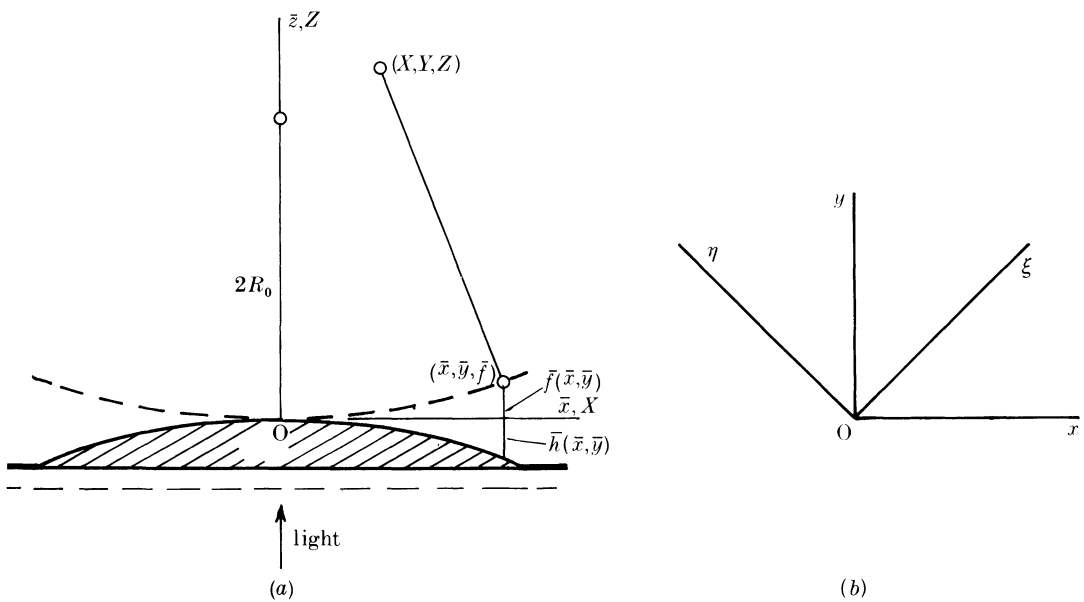


FIGURE 1. (a) Coordinate system seen in the vertical plane. The water drop is shaded and the incoming and outgoing wavefronts are shown by the broken lines. Coordinates $(\bar{x}, \bar{y}, \bar{f})$ denote a general point on the outgoing wavefront, while (X, Y, Z) is a general point in the caustic space. (b) Axes in the horizontal tangent plane to the drop at O .

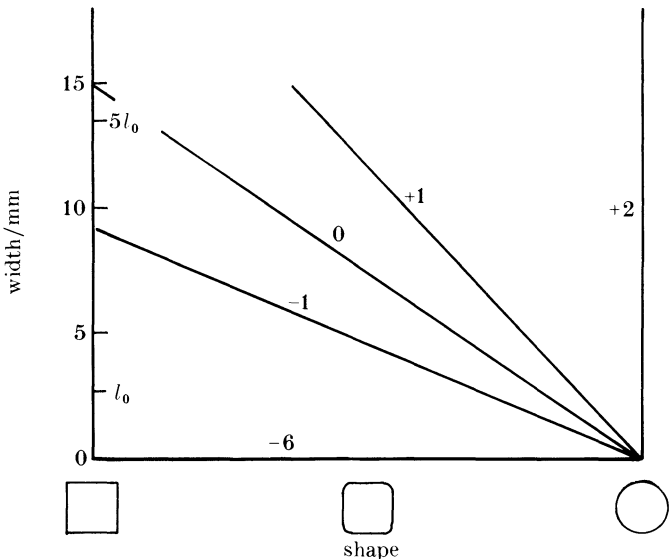


FIGURE 2. Schematic diagram to show the effect on the modulus K of the width and shape of the aperture. The numbers on the lines are values of K . This is for thin drops resting on the upper surface of the glass slide.

(Facing p. 6)

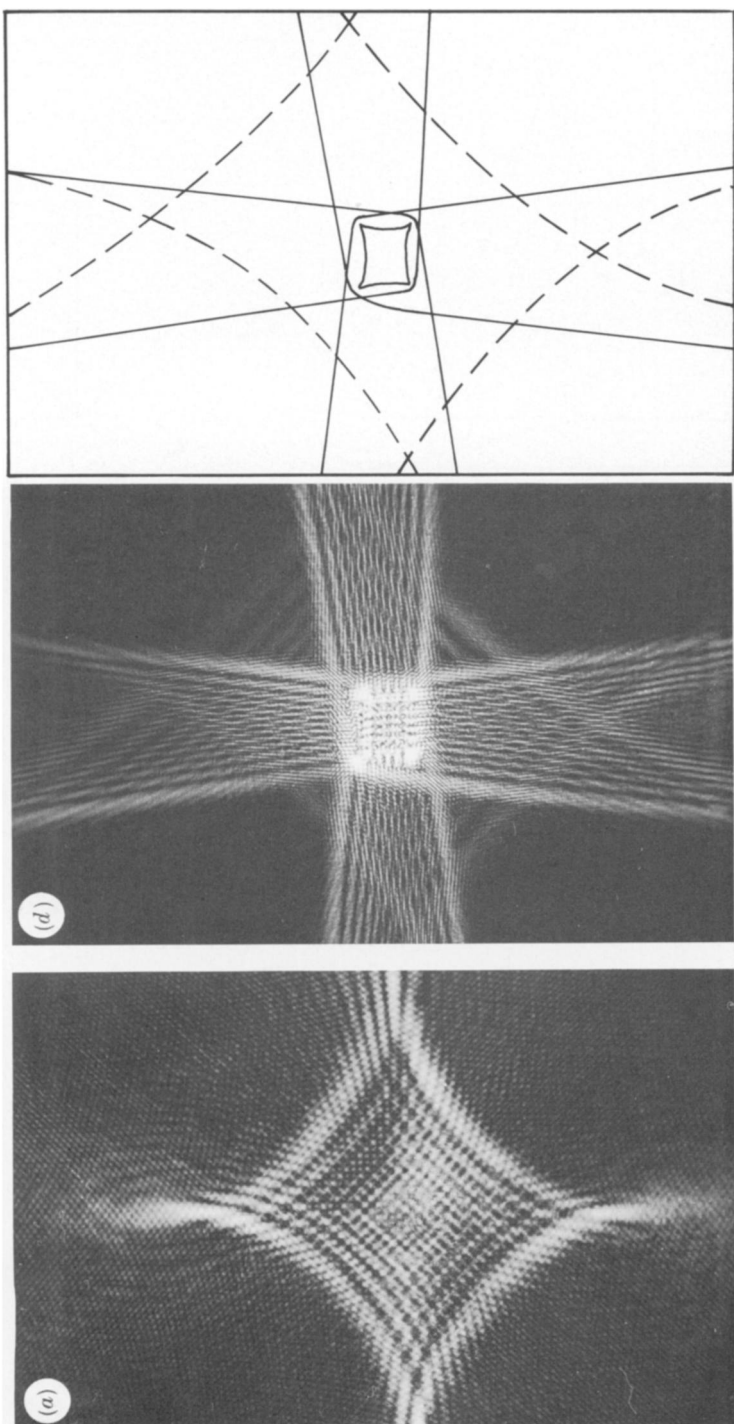


FIGURE 3a, d, Diagrams (a)–(c) and (d)–(f) are focusing sequences moving downwards towards the drop. For (a)–(c) K is close to -6 . For (d)–(f) more water has been added and K is slightly less than 0 .

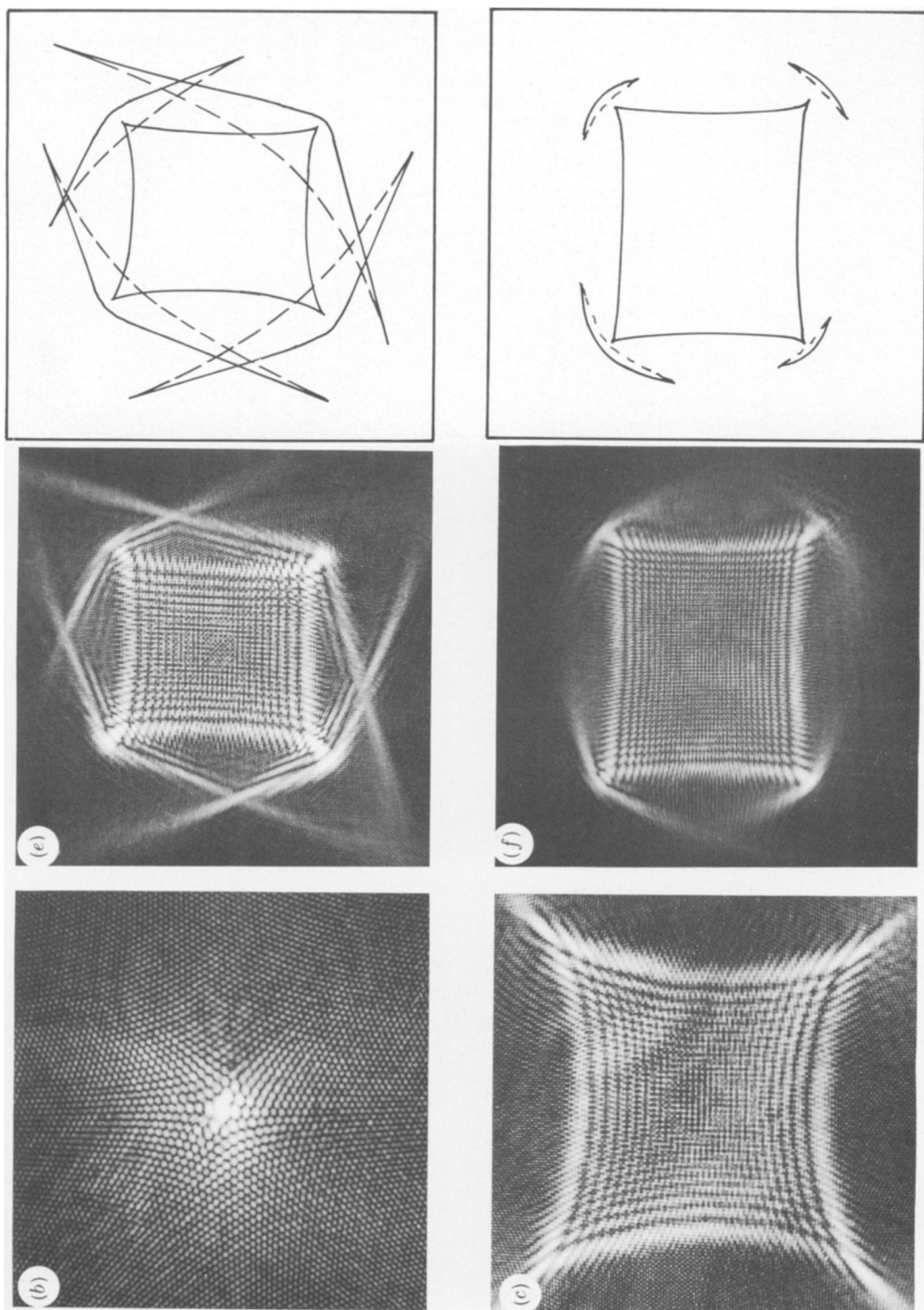


FIGURE 3*b, c, e, f*. For description see above.

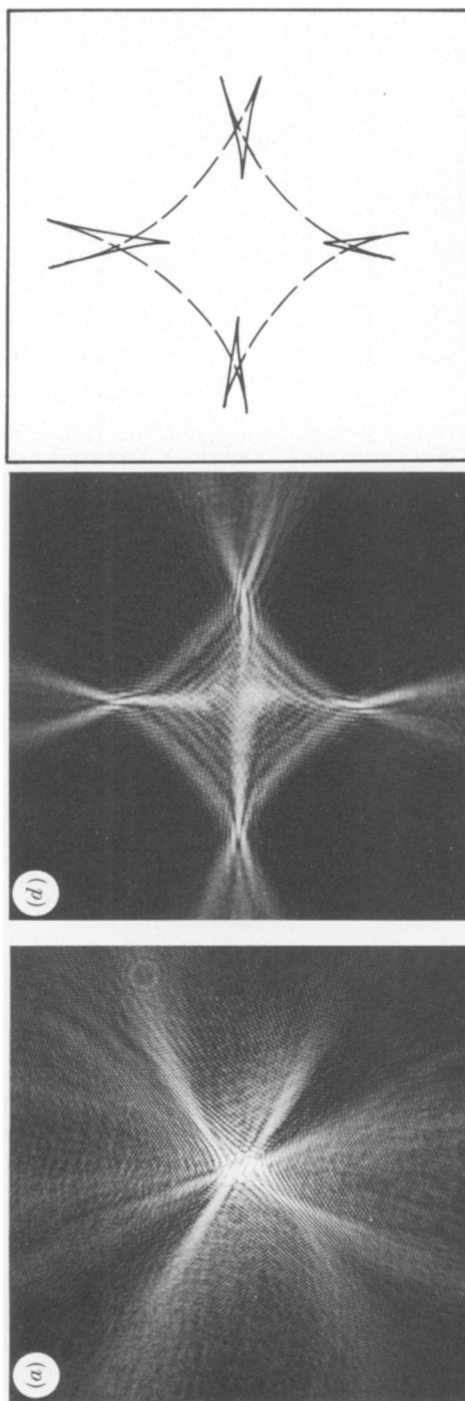
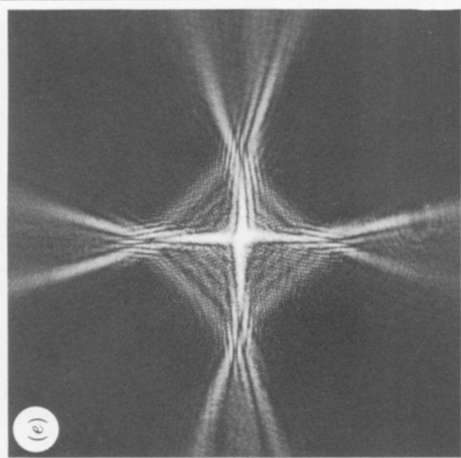
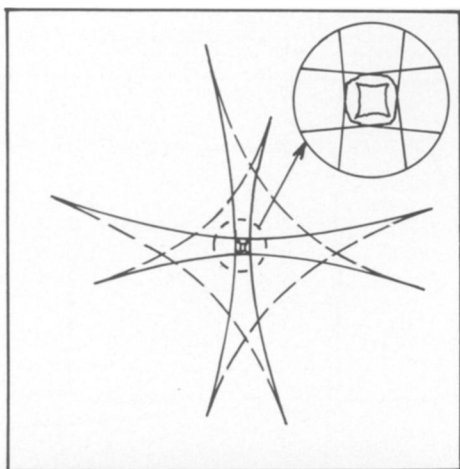
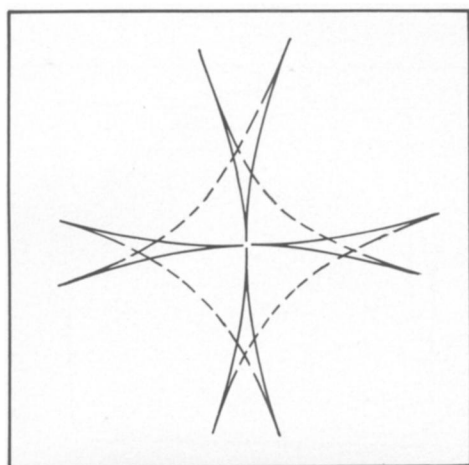
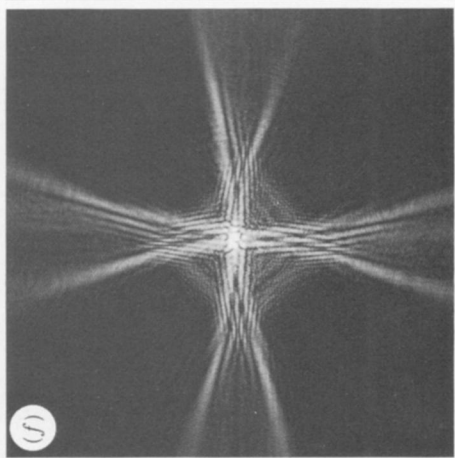


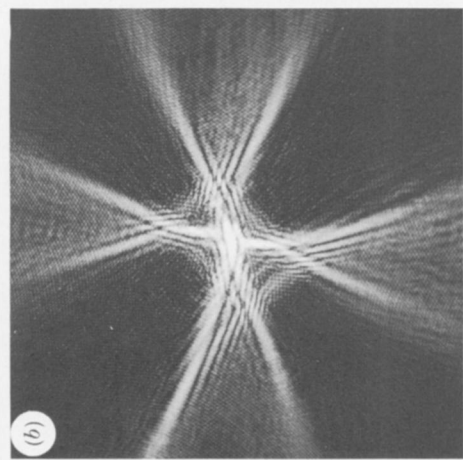
FIGURE 4a, d. These patterns, where K is between -2 and 0 , may be compared with figure 9. (a) Close to $K = -2$, $W_3 = 0$, a highly unstable pattern dominated by diffraction, but very different from figure 3b. (b), (e) Also have $W_3 \approx 0$ and are like the second and third diagrams of figure 9. (c) $W_3 < 0$ (compare figure 7m). (d), (e), (f) The same value of K but decreasing values of W_3 , as in figures 7i, j, k; note how the fainter diagonal folds, which are not part of X_g , move inwards, but do not reach the centre at $W_3 = 0$. In (f) the inferred detail is lost in the diffraction, but it emerges in figure 3d.



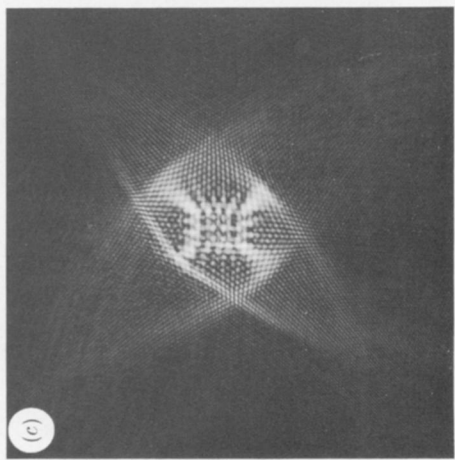
(e)



(f)



(g)



(c)

FIGURE 4b, c, e, f. For description see above.

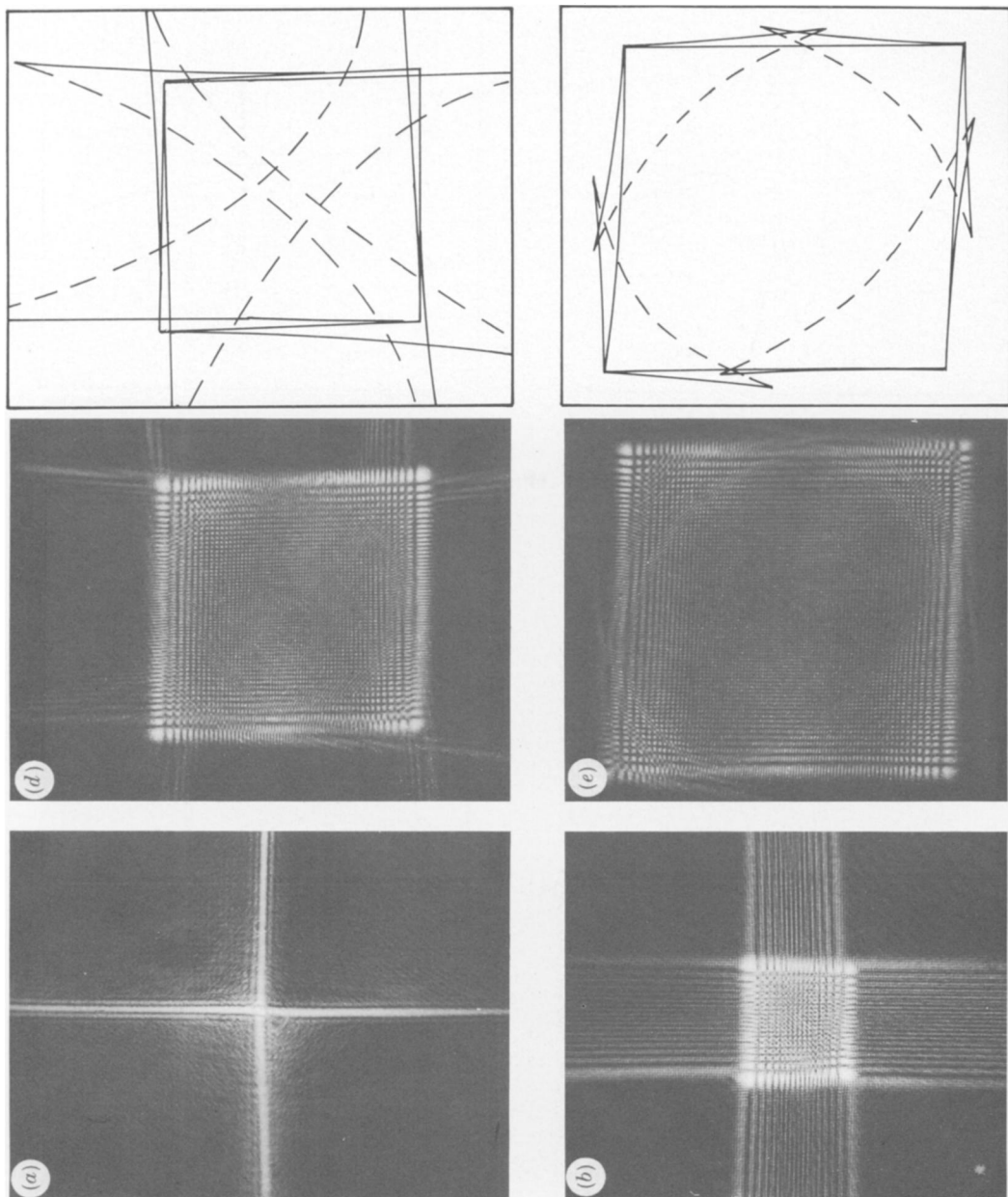


FIGURE 5a, b, d, e. For description see below.

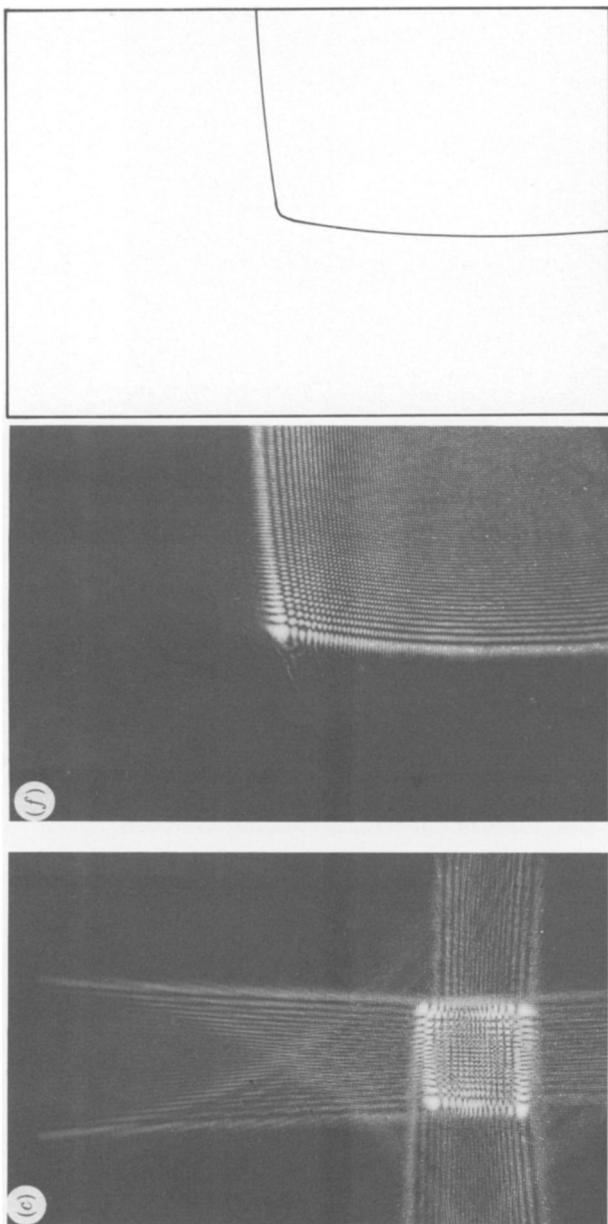


FIGURE 5c,f. In (a)-(f), a sequence moving downwards is shown, starting at the focus with $K = 0$, and keeping on the umbilic locus by adding water. Thus K increases slightly through the sequence. Four hyperbolic foci are seen until (f) when they become parabolic, as is confirmed by the characteristic diffraction pattern at each corner of the figure. The hole size is not critical and varies between 3.2 and 4.6 mm in this sequence.

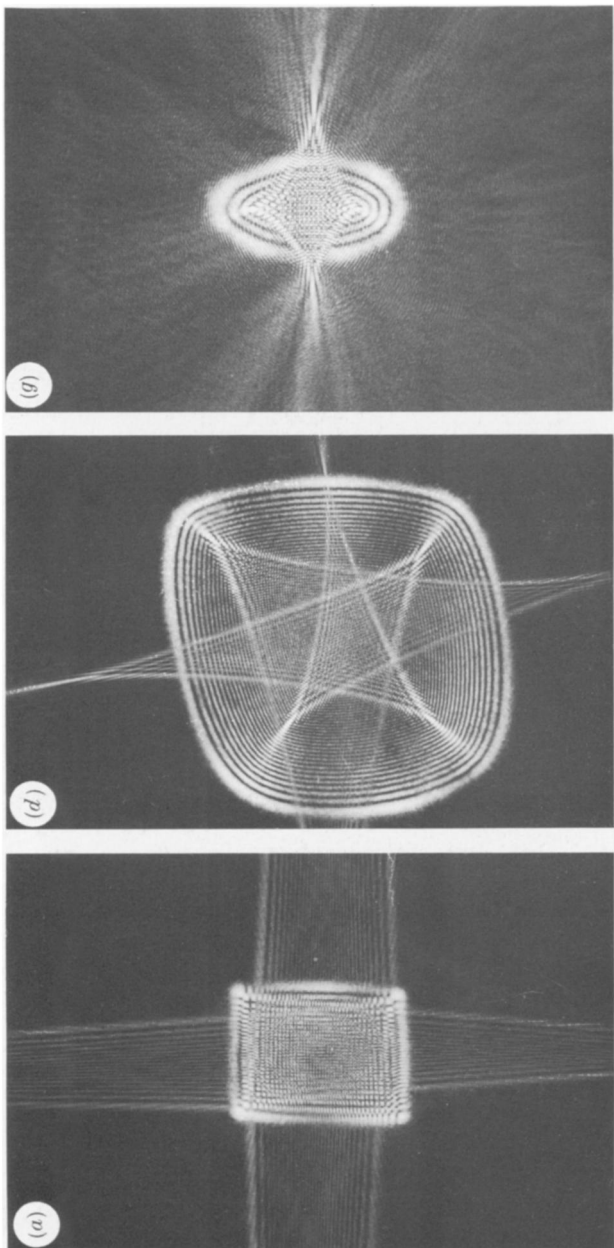


FIGURE 6*a,d,g.* K is between 0 and 2, and $W_3 < 0$. (*a*) Close to the hyperbolic umbilic locus and on the side of high K ; the hyperbolic umbilics are slightly unfolded; compare with figure 7*r*. (*b*, (*c*) Higher values of K , with W_3 lower in (*c*). (*d*) A still higher value of K so that the 8-cusped figure approaches 8-fold symmetry. (*e*) Approximate 3m symmetry that comes from a nearly circular hole of diameter 5.8 mm, having three hardly perceptible nicks in its boundary; there are 6 cusps alternately inside and outside the oval caustic. (*f*) From an unsymmetrical drop. (*g*) For 2mm symmetry (compare figure 21*b*). In (*h*) and (*i*) the symmetry is broken from 2 mm to approximately m. (*f*)–(*i*) From drops that have transgressed the edges of the square hole.

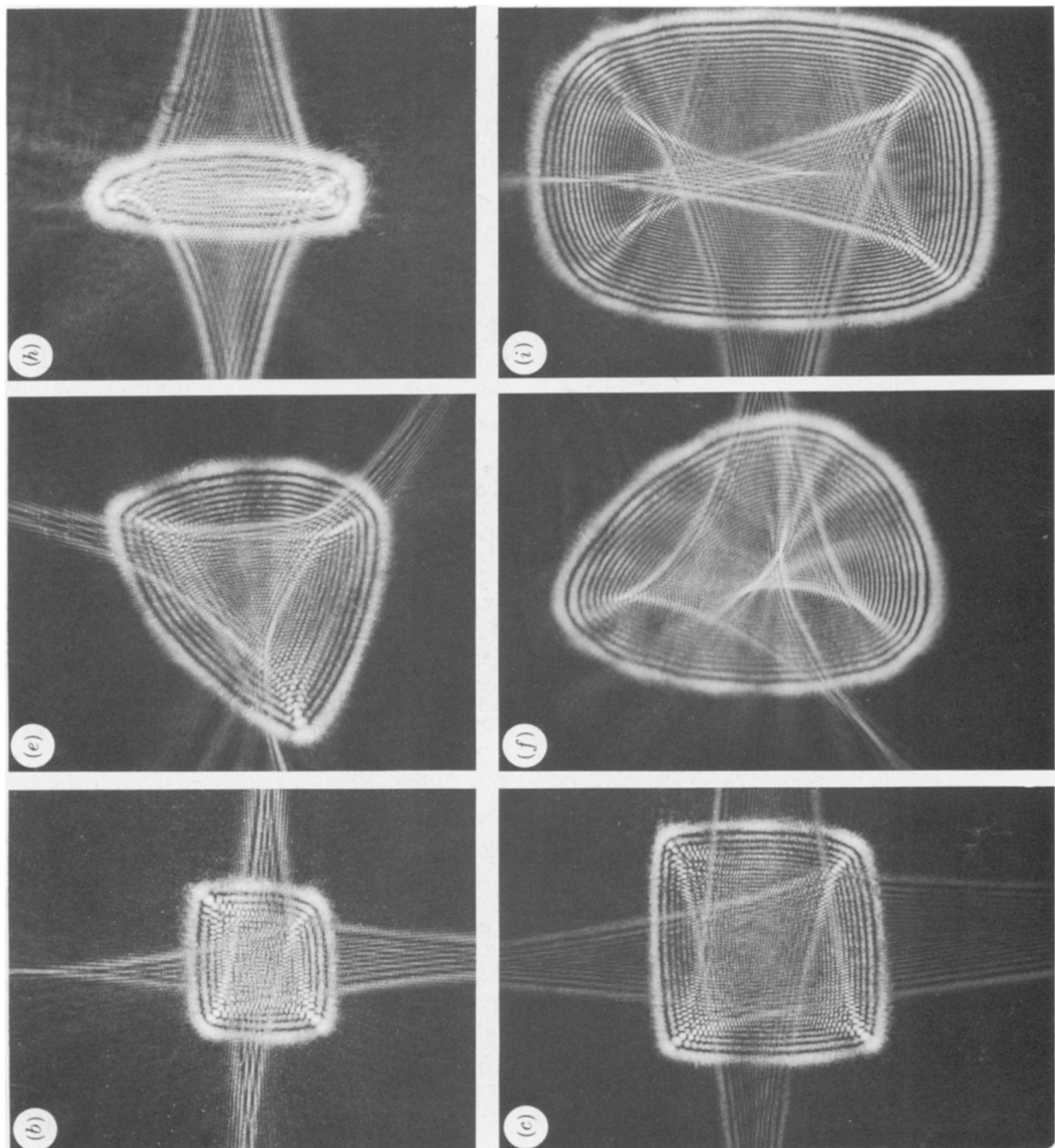


FIGURE 6b, c, e, f, h, i. For description see above.

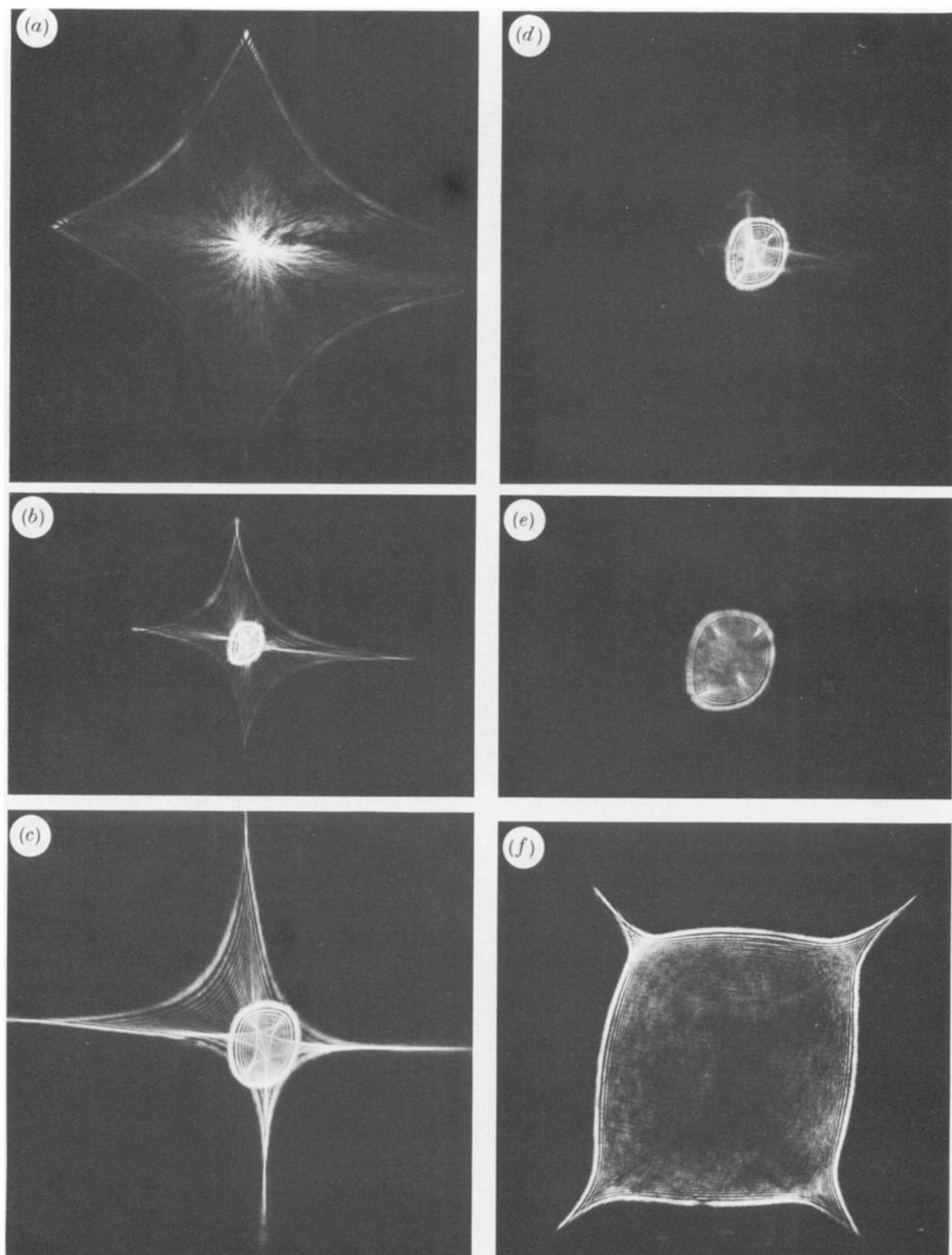


FIGURE 18. Caustics formed by a water drop clinging to the *lower* surface of a glass slide and illuminated from below. The hole was a square with side 7.3 mm and it was filled to produce a focal length $2R_0 = 6$ mm. The sequence (a)–(f) starts at the focus and moves downwards, towards the drop. The whole sequence is similar to, but not identical with, that of figure 14; that is, standard X_9 patterns with K slightly greater than zero. Note the different shape of the 4-cusped caustic in (f) and in figure 14b.

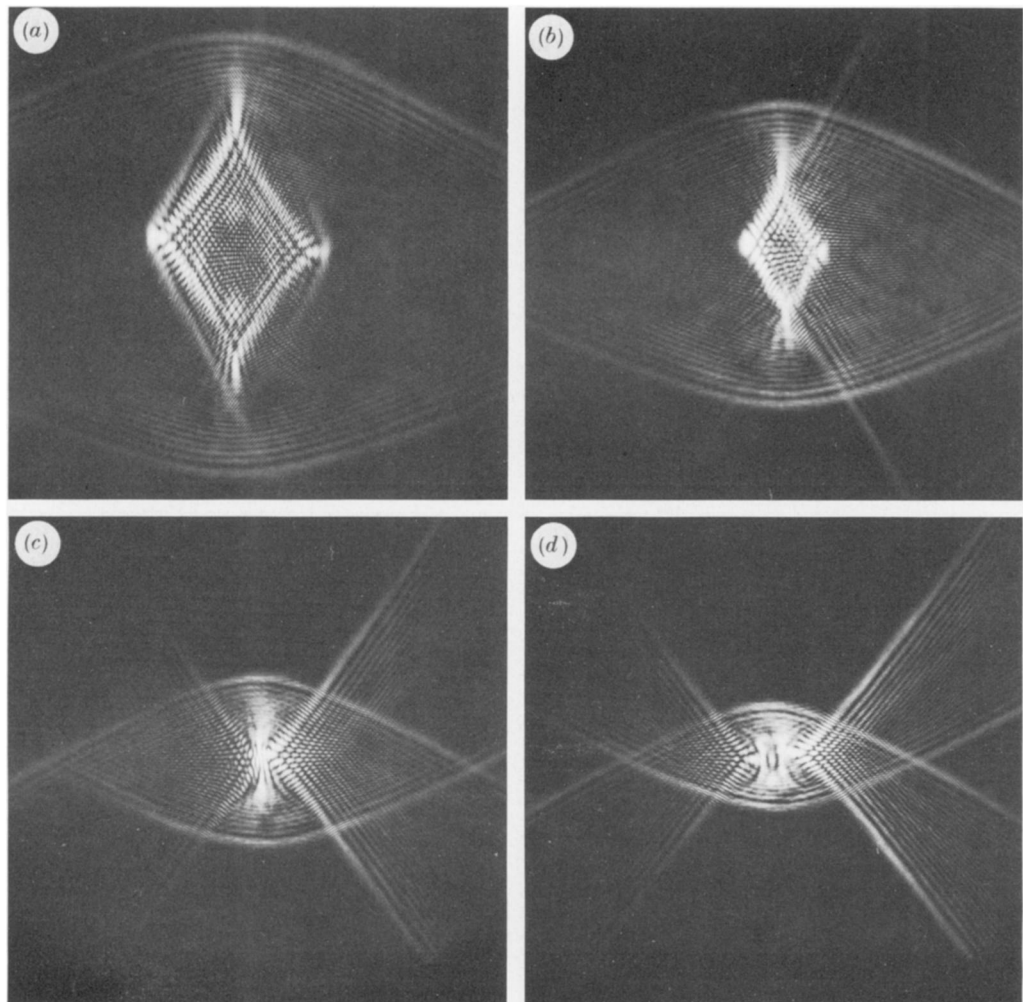


FIGURE 19a-d. (a)–(g) As for figure 18, focusing downwards, but the hole was slightly rectangular, 9.0 mm \times 8.9 mm. In (d) two parabolic umbilic foci are seen, point to point. (h) The same, but from a square hole of side 7.3 mm; the pattern is below the focus of the drop and the cusps move outwards as the microscope is lowered. Compare with figure 4b, in which the cusps move outwards as the microscope is raised. Thus the sequence is inverted and turned through 45°.

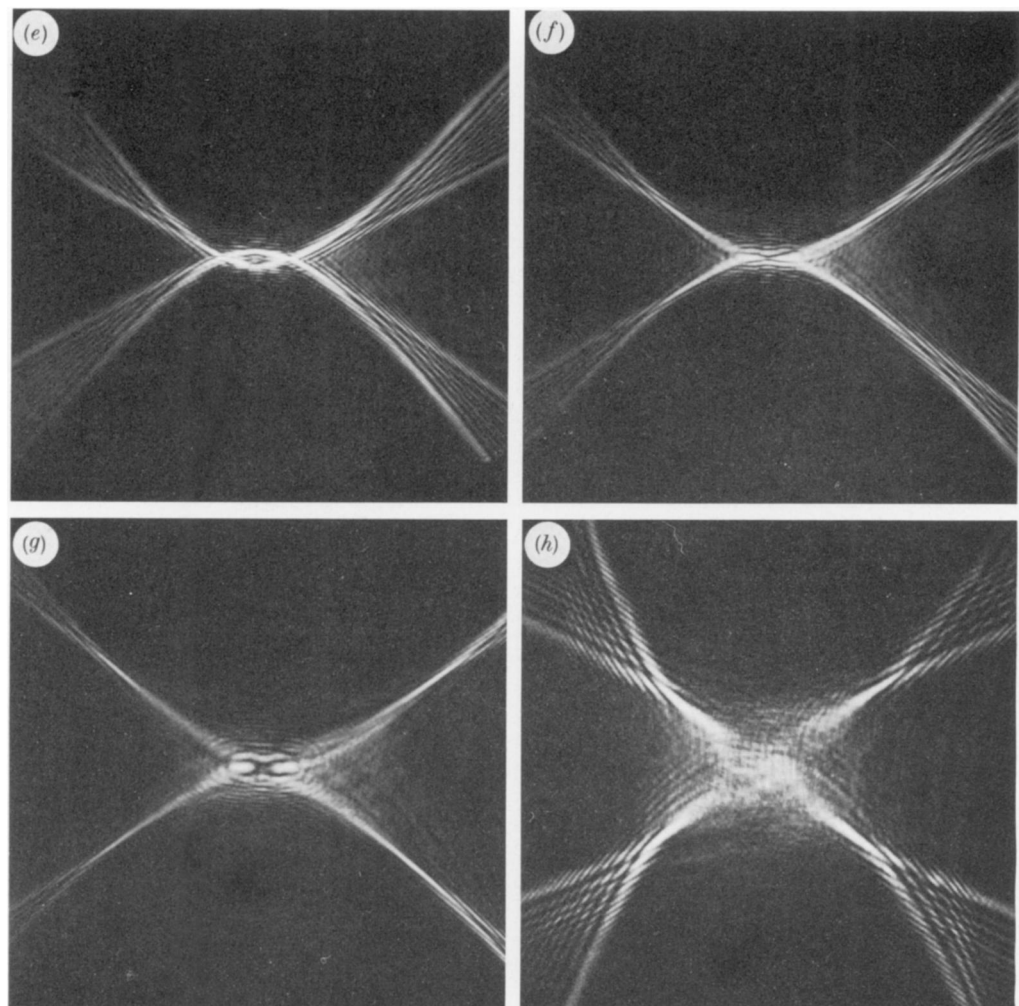


FIGURE 19*e–h*. For description see plate 10.

the wavefront of (10), equation (13) is now

$$\begin{aligned}\phi(x, y; W_1, W_2, W_3) = & x^4 + Kx^2y^2 + y^4 + Ax^6 + Bx^4y^2 + Bx^2y^4 + Ay^6 \\ & + W_3(x^2 + y^2) + W_2y + W_1x + O(8),\end{aligned}\quad (16)$$

A and B being given in terms of K by

$$A = \left(\frac{l}{l_0}\right)^2 \frac{12-K}{360}, \quad B = \left(\frac{l}{l_0}\right)^2 \frac{K}{24}.$$

The germ of ϕ , that is $\phi(x, y; 0, 0, 0)$, is

$$x^4 + Kx^2y^2 + y^4 + O(6).$$

The higher order terms may be transformed away by the usual rules for equivalence and we recognize the germ of X_9 given in §1, provided $K \neq \pm 2$. So we now know, from the principles of catastrophe optics, that if $K \neq \pm 2$, the wavefront (10) will produce caustics corresponding to an unfolding of the catastrophe X_9 .

Before looking at the details of the caustics we must say something about the approximations that have been made, because they might have robbed the calculated higher order terms of all significance. There have been three approximations: (i) the use in (1) of an approximate formula for curvature, (ii) the use of the linearized form of Snell's law (2), and (iii) the use of a generating function (13) that gives the ray directions only approximately. All three approximations derive from the assumption of small slopes. This refers, of course, to $\partial f/\partial \bar{x}$, $\partial f/\partial \bar{y}$ and not to the non-dimensional $\partial f/\partial x$, $\partial f/\partial y$, for the condition is (taking $l = l_0$)

$$\frac{l_0}{R_0} \frac{\partial f}{\partial x} \ll 1, \quad \frac{l_0}{R_0} \frac{\partial f}{\partial y} \ll 1.$$

If we take any solution of the differential equation (5), subject to $f = 0$ and $\partial f/\partial x = \partial f/\partial y = 0$ at the origin, and choose one of its level curves as the boundary, this single solution will represent a range of drops of different thicknesses according to the value assigned to R_0 (notice that in (3), \bar{f} scales with $1/R_0$). Thus, by choosing R_0 large enough, the slopes may be made as small as we like. This means that the higher order terms in our wavefront expressions are indeed correct, provided R_0 is sufficiently large. The essential point is that, while \bar{x} and \bar{y} scale with l_0 , the slopes scale with l_0/R_0 .

4. CAUSTICS ORGANIZED BY X_9 AND BY $Y_{2,2}^1$

Some representative caustics photographed through a microscope are shown in figures 3 (plates 1 and 2), 4 (plates 3 and 4), 5 (plates 5 and 6), 6 (plates 7 and 8), and diagrammatically, ignoring the inevitable diffraction, in figure 7. Figures 3–6 show caustics from water drops resting on the upper surface of a horizontal glass slide and illuminated from below. The drops rest in square holes of sides between 3.2 and 4.6 mm, the sides of the holes being parallel to the edges of the photographs (figure 6e is an exception). The width of the field of view is typically 0.7 mm. The technique was similar to that used in previous studies (Nye 1978, 1979). The drop

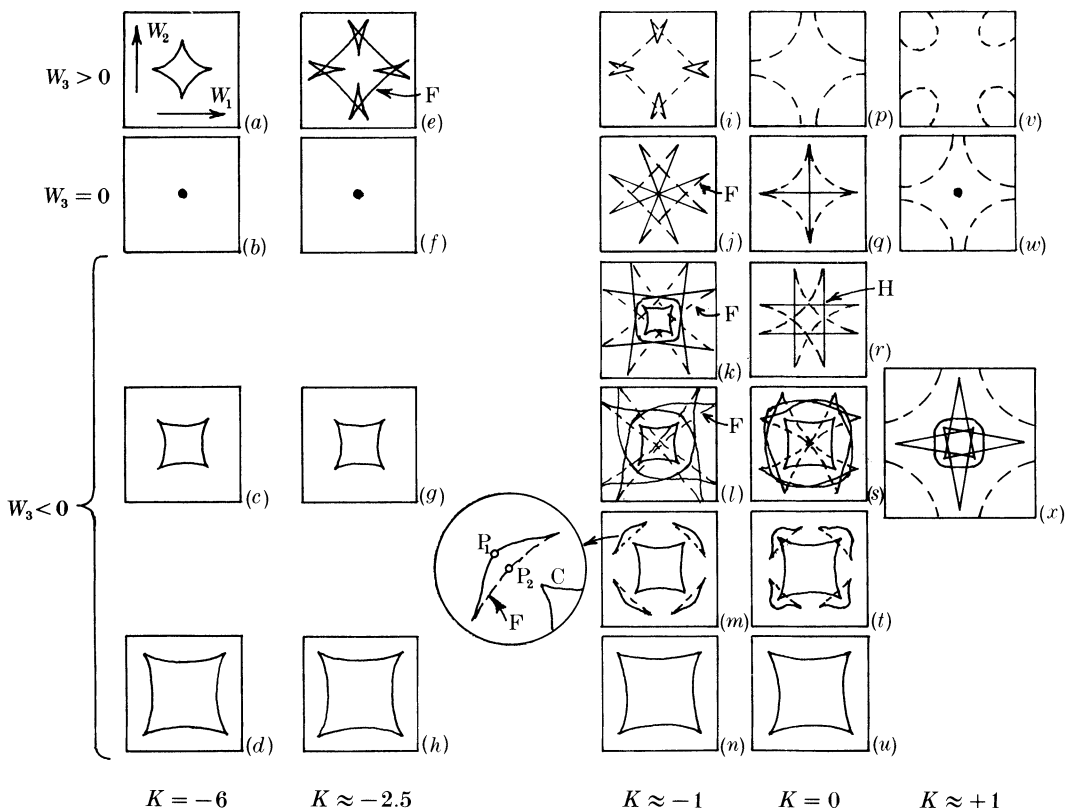


FIGURE 7. Sketches of caustics, only approximately to scale, summarizing the observations of figures 3–6. Each box shows a caustic in (W_1, W_2) and the boxes are arranged in the space (K, W_3) . Thus a column represents a focusing sequence.

was illuminated from below by a broadened parallel laser beam reflected from a surface-silvered mirror, and the caustics in the space above the drop were observed and photographed through a microscope, by using an 8 mm objective (numerical aperture = 0.5). It was essential to protect the microscope from vibration. The diagrams in figure 7 are arranged on a coordinate system (K, W_3) : coordinate K corresponds to building up the drop (droplet by droplet from a hypodermic needle) or thinning it (sucking with the needle, or allowing it to evaporate) in a fixed square aperture, while W_3 corresponds to raising and lowering the microscope with the focusing control. For each (K, W_3) there is a caustic pattern in the horizontal plane, with coordinates W_1, W_2 ; these are shown in the individual boxes. K ranges from -6 to 2 , as previously discussed, while W_3 ranges about zero, the height of the centre of curvature of the wavefront. Figure 8a provides a key to the photographs, showing roughly their relative locations in (K, W_3) space.

Each observed caustic pattern is accompanied by characteristic diffraction. Apart from this the patterns are exactly what would be expected from theoretical and numerical studies of X_9 (Callahan 1982a; Upstill 1979), but with the addition

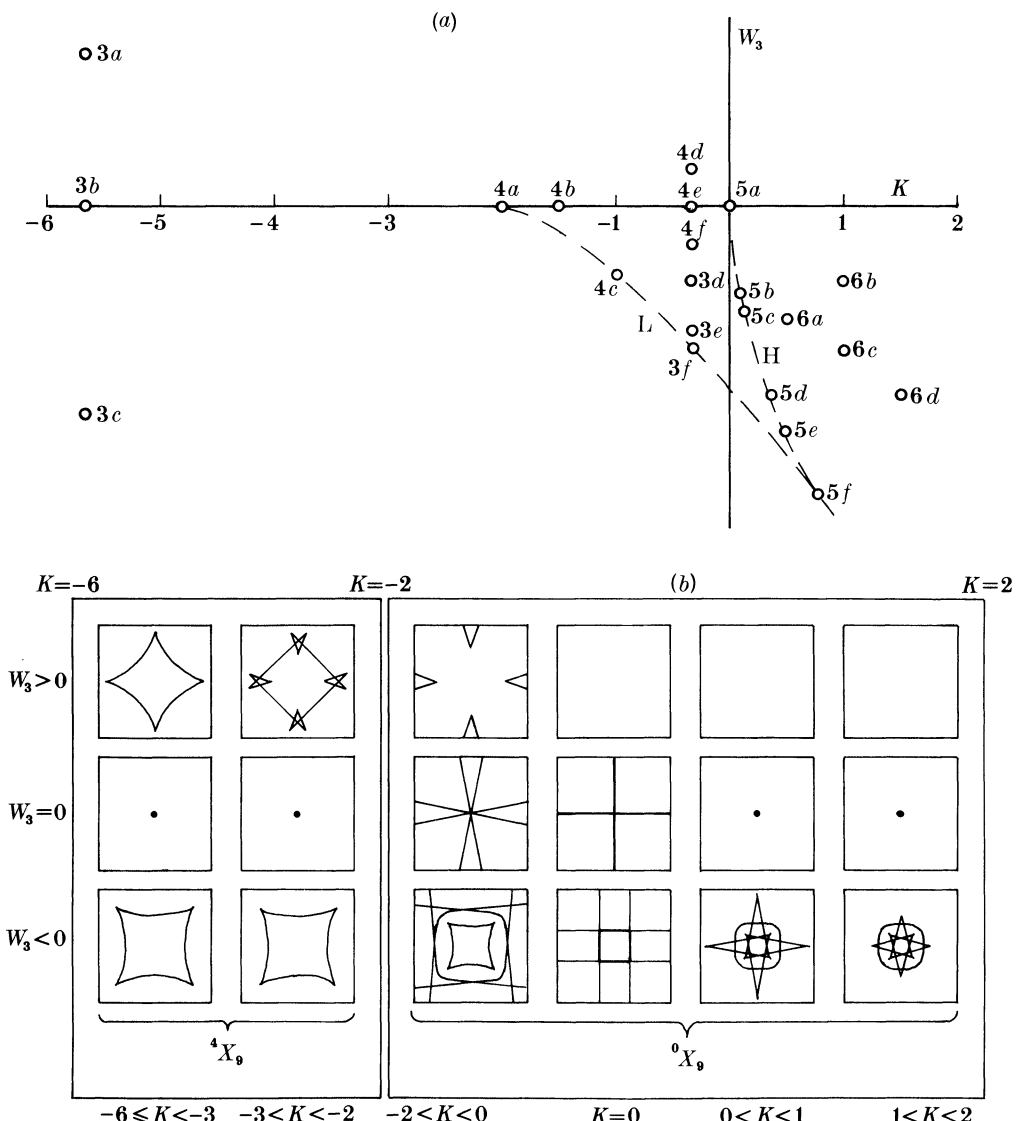


FIGURE 8. (a) Key to photographs in figures 3–6. The points, labelled with the figure numbers, show roughly the position of each figure in (K, W_3) space. L = lips locus, H = hyperbolic umbilic locus. (b) The caustics organized by X_9 alone arranged as in figure 7.

of certain conspicuous extra fold lines, which are shown by broken lines. We shall see that these are associated with the higher catastrophe $Y_{2,2}^1$ in which X_9 is here embedded. Although the patterns were obtained by using a square hole, this was not essential. Up to order 4 in the expression (16) for ϕ there is only one parameter, K , that is not fixed by the governing differential equation. Therefore we expect the same X_9 unfoldings for all apertures with the same symmetry as a square. The structural stability hereby exhibited even extends, as we mentioned above, to the

caustics from highly curved drops where the assumptions of the detailed small-slope analysis break down.

To explain the extra folds (broken lines) we must include sixth-order terms in the wavefront. First transform to new axes (figure 1*b*) turned through 45° about $O\bar{z}$: thus $(x, y) \rightarrow (\xi, \eta)$. Then the generating function ϕ in (16) takes the form (with $l = l_0$)

$$\begin{aligned}\phi'(\xi, \eta; W'_1, W'_2, W'_3) &= \kappa\xi^4 + \xi^2\eta^2 + \kappa\eta^4 + \alpha\xi^6 + \beta\xi^4\eta^2 + \beta\xi^2\eta^4 + \alpha\eta^6 \\ &\quad + W'_3(\xi^2 + \eta^2) + W'_2\eta + W'_1\xi + O(8),\end{aligned}\quad (17)$$

where we have divided by $\frac{1}{2}(6-K)$ to make the coefficient of $\xi^2\eta^2$ unity and W'_1, W'_2, W'_3 are controls parallel to ξ, η and Z . The coefficients on these 45° axes are denoted by greek letters. The coefficient κ now plays the role previously played by K , the relation being

$$\kappa = (2+K)/2(6-K), \quad (18)$$

and so κ increases through zero as K increases through -2 (a value forbidden to X_9). The sixth-order coefficients α and β are fixed through the governing differential equation (5) as

$$\alpha = \frac{1}{360}(12\kappa - 1), \quad \beta = \frac{1}{24}. \quad (19)$$

In X_9 , κ is a modulus and not a control, because varying κ does not produce lower order critical points, but merely other members of the X_9 family. However, in the sixth-order germ that we now have, varying κ to produce the unfolding term $\kappa(\xi^4 + \eta^4)$ does produce lower order critical points, namely a member of X_9 . Therefore, we now treat κ as an additional control variable. The germ of (17), obtained by putting $\kappa = W'_1 = W'_2 = W'_3 = 0$, is

$$\xi^2\eta^2 + \alpha\xi^6 + \beta\xi^4\eta^2 + \beta\xi^2\eta^4 + \alpha\eta^6 \quad (\alpha < 0),$$

the $O(8)$ terms being removable by suitable transformation. Since α is negative for $\kappa = 0$ we change the sign of the whole expression (for the sign is of no significance in optics) and then scale ξ and η to obtain the form

$$-\xi^2\eta^2 + \xi^6 + \beta'\xi^4\eta^2 + \beta'\xi^2\eta^4 + \eta^6.$$

The transformations $\xi \rightarrow \xi(1 + \beta'\xi^2)^{\frac{1}{2}}$, $\eta \rightarrow \eta(1 + \beta'\eta^2)^{\frac{1}{2}}$, absorb the terms in $\xi^4\eta^2$ and $\xi^2\eta^4$ into $-\xi^2\eta^2$, creating additional $O(8)$ terms, which are removable. We are left with

$$\xi^6 - \xi^2\eta^2 + \eta^6.$$

This is the germ of the catastrophe denoted by Arnold (1975) as $Y_{2,2}^1$, namely $x^6 + a_0x^2y^2 + y^6$ ($a_0 \neq 0$) with the modulus $a_0 = -1$.

Thus, features of the caustic pattern that depend essentially on sixth-order terms in the wavefront are organized by this higher singularity. To distinguish those features that are part of the local unfolding of X_9 from those that are global to it and organized by $Y_{2,2}^1$ we show the X_9 unfoldings separately in figure 8*b*.

Looking first at the level $W_3 = 0$, we see that it contains simply a point focus, except for the range $-2 < K < 0$ where four lines appear. To examine this keep only the fourth-order terms in the germ of (16) and find the fold locus on the wavefront, for which the condition is $\phi_{xx}\phi_{yy} - \phi_{xy}^2 = 0$ (subscripts denote differen-

tiation). Putting $W_3 = 0$ yields straight lines $x^2 = ky^2$, where k is a double-valued constant determined by K ,

$$k = [K^2 - 12 \pm \sqrt{\{(36 - K^2)(4 - K^2)\}}]/4K,$$

and where $-2 < K < 0$ (or $K > 6$), as expected. The corresponding locus in (W_1, W_2) is obtained by using the mapping $(x, y) \mapsto (W_1, W_2)$ resulting from the ray condition $\phi_x = \phi_y = 0$. This gives the four lines

$$\frac{W_1}{W_2} = \pm k \left(\frac{2k + K}{2 + Kk} \right).$$

In the limit $K \searrow -2$, $W_1/W_2 \rightarrow 1$ and so the folds are at 45° to the axes, while for $K \nearrow 0$, $W_1/W_2 \rightarrow 0$ and ∞ . Thus the *slopes* of the four lines are explained by X_9 . But a conspicuous feature of the observations (figure 4, shown diagrammatically in figure 9) is that the *lengths* of the lines become zero as $K \searrow -2$. The reason is that they are terminated by folds (broken lines) belonging to $Y_{2,2}^1$ and these pass through $W_1 = W_2 = W_3 = 0$, that is, become local, precisely at $K = -2$, thus extinguishing the X_9 folds.

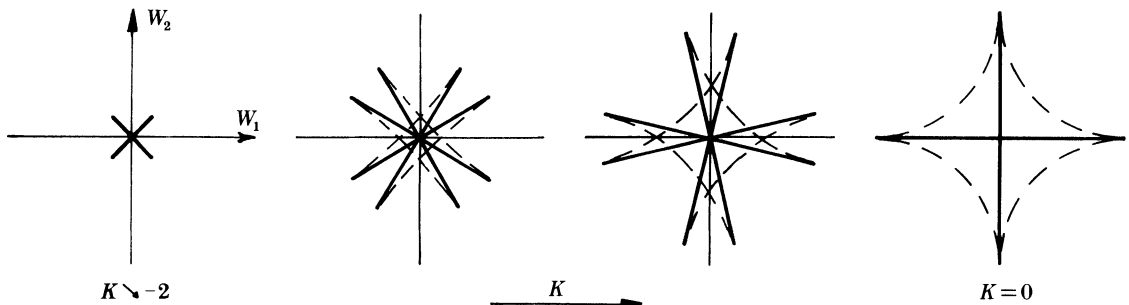


FIGURE 9. Caustics in the plane $W_3 = 0$ for $-2 < K \leq 0$ organized by X_9 and (broken lines) by $Y_{2,2}^1$.

5. CRITICAL POINTS ON THE WAVEFRONT CORRESPONDING TO CONTROL POINTS ON THE W_3 AXIS

In this section we show in more detail how the sixth-order terms in the wavefront expression, associated with $Y_{2,2}^1$, are necessary to explain the observed caustics. For this purpose consider the feet of the rays passing through points on the W_3 axis near to $W_3 = 0$. These are the critical points in (x, y) , or the blossom. Since x and y are small, we at first keep only the lowest order terms in expression (16) for ϕ :

$$\phi(x, y; 0, 0, W_3) = x^4 + Kx^2y^2 + y^4 + W_3(x^2 + y^2).$$

The ray conditions $\phi_x = \phi_y = 0$ give

$$x = 0 \quad \text{or} \quad 2x^2 + Ky^2 = -W_3, \quad \left. \right\}$$

with

$$y = 0 \quad \text{or} \quad 2y^2 + Kx^2 = -W_3, \quad \left. \right\}$$

which represents the intersections of two loci, each consisting of a straight line and a central conic (ellipse or hyperbola) parametrized by (K, W_3) . All the possibilities are shown by the dots in figure 10a. Generally there are 1, 5 or 9 rays, but the cases $K = -2$, $W_3 = 0$ and $K = 2$, $W_3 \leq 0$ are exceptional because parts of the two loci coincide, making the intersections indeterminate. Clearly, terms of higher order are needed to resolve these indeterminacies: in fact sixth order for the first and eighth order for the second.

To deal with the case $K = -2$, $W_3 = 0$ we write down (16) up to sixth order and include the new terms in the ray conditions. A short calculation then shows that the corrected loci near $K = -2$, $W_3 = 0$ are as in figure 10b. The indeterminacy at $K = -2$, $W_3 = 0$ is resolved to yield a single critical point at $(x, y) = (0, 0)$, but near $K = -2$, $W_3 = 0$ four new intersections (open circles) appear, to bring the maximum number of critical points to 13, which is the multiplicity of $Y_{2,2}^1$. These new critical points recede to infinity as $K \rightarrow -\frac{6}{7}$, which corresponds on 45° axes to $\alpha = 0$. (W_3 is assumed small in this analysis but K need not be near -2 .) The lower right diagram shows how the old and new critical points merge when

$$W_3 = 15(2+K)^2/(6+7K) \quad (K \approx -2).$$

This event, which is obviously not part of X_9 , corresponds to a fold sweeping through the centre ($W_1 = W_2 = 0$) of the caustic pattern. The fold in question is F in figure 7m, l and k; the transition between (m) and (k), although dramatic, is simply the growth of the four small lips in (m) to become the four large lips in (k). As confirmation that this fold is not part of X_9 we may note that when $W_3 = 0$, for fixed $K > -2$, it does not pass through the centre $W_1 = W_2 = 0$.

On the other hand, when $K < -2$ figure 7e shows that this same fold F does pass through the centre as $W_3 \searrow 0$, and is part of X_9 . To see how this comes about we may use the 45° axes $O\xi, O\eta$, consider the fold locus $\phi'_{\xi\xi}\phi'_{\eta\eta} - \phi'^2_{\xi\eta} = 0$, and examine its intersections with $\eta = 0$. Then $\phi'_{\xi\eta} = 0$, which implies $\phi'_{\xi\xi} = 0$ or $\phi'_{\eta\eta} = 0$. The solution $\phi'_{\eta\eta} = 0$ corresponds to cusps such as C (figure 7m); we need the solution $\phi'_{\xi\xi} = 0$, which is

$$\phi'_{\xi\xi} = 15\alpha\xi^4 + 6\kappa\xi^2 + W'_3 = 0. \quad (20)$$

Near $\kappa = 0$ ($K = -2$) relations (19) show that $\alpha < 0$. So $\phi'_{\xi\xi}$ as a function of ξ for fixed W'_3 is as shown in figure 11a-d. The roots P_1, P_2 are the folds shown by the corresponding letters in figure 7m. For $\kappa > 0$, as W'_3 becomes more negative figure 11d shows that the roots merge to give lips; but as W'_3 increases through zero the inner root P_1 is lost and only the outer root P_2 (arising from the quartic term in (20), i.e. from $Y_{2,2}^1$) survives. For $\kappa < 0$ ($W'_3 > 0$) this root is still present, but now it arises from the quadratic term, i.e. from X_9 . Notice how, for $\kappa < 0$ root P_2 comes to the origin as $W'_3 \rightarrow 0$, while for $\kappa > 0$ it does not. This explains the change in parentage of the fold F as K passes through -2 .

It is evidently the sign of α that decides the presence of the outer roots; it is significant that it also decides whether the modulus a_0 of $Y_{2,2}^1$ is $+1$ or -1 . Since the sign of α is fixed by the governing differential equation, rather than by the boundary conditions, it is the differential equation that decides which modulus of $Y_{2,2}^1$ is applicable.

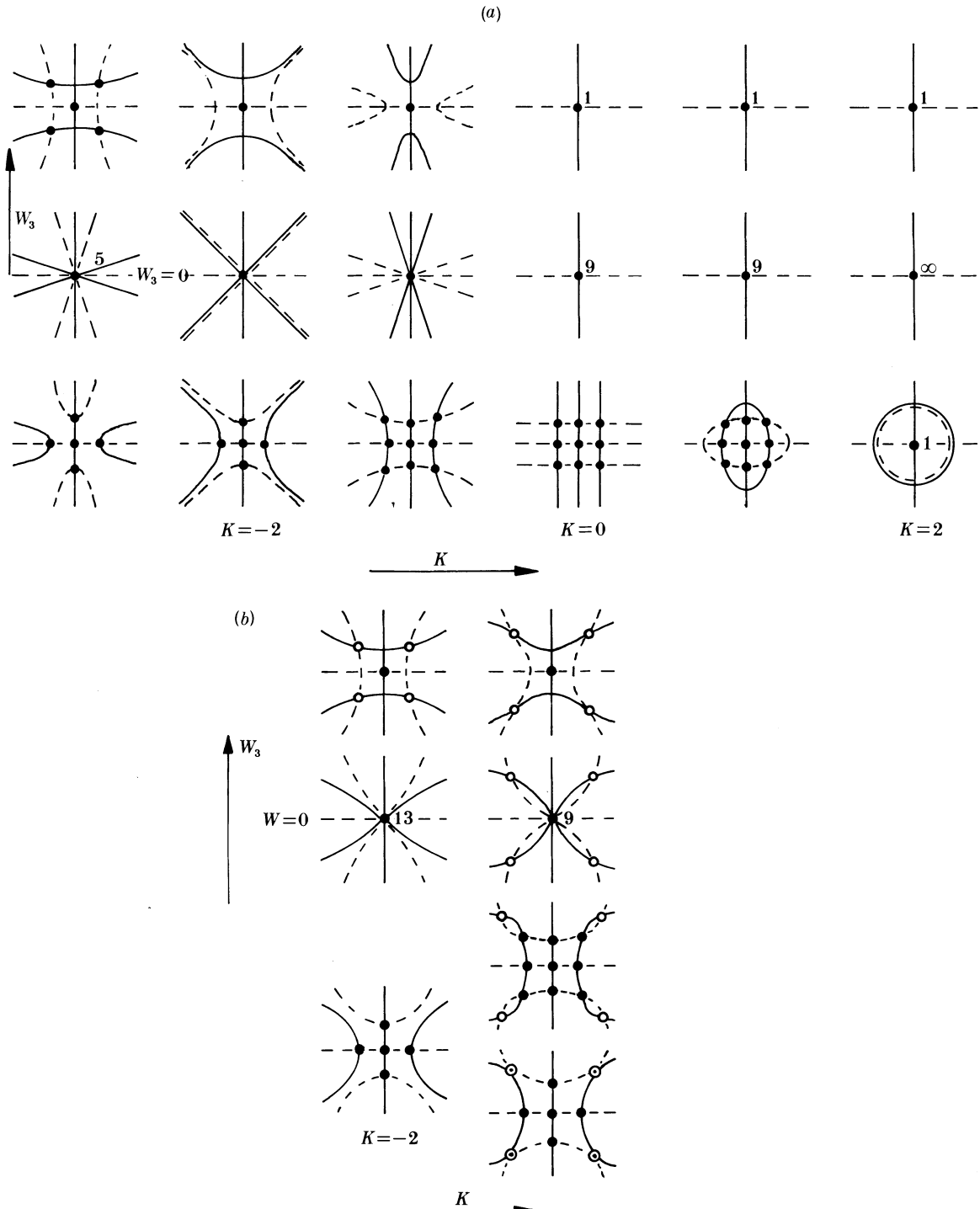


FIGURE 10. (a) Critical points for X_9 . Each sketch shows the critical points in (x, y) and the sketches are arranged on coordinates (K, W_3) . The numbers show the multiplicity. (b) Critical points in (x, y) for $K = -2$ and K slightly greater than -2 , showing how $Y_{2,2}^1$ resolves the indeterminacy of X_9 at $K = -2$, $W_3 = 0$, and produces extra critical points non-local to X_9 . ● Old (X_9) points; ○, new ($Y_{2,2}^1$) points; ⊖, merging of old and new.

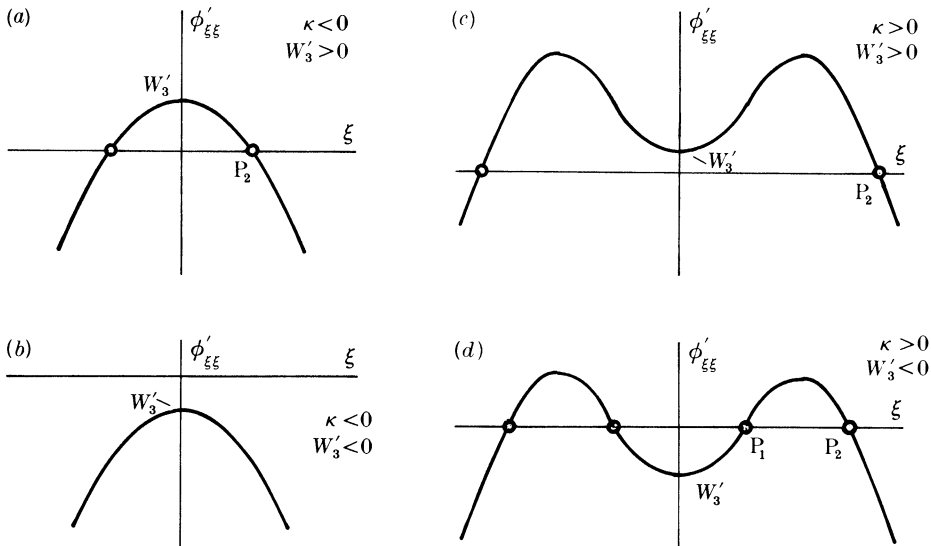


FIGURE 11. The function $\phi'(\xi)$ on $\eta = 0$ showing the behaviour of the roots of $\phi'(\xi) = 0$ in the neighbourhood of $\kappa = 0$ ($K = -2$) and $W_3' = 0$.

We see from the above that the lips locus in (K, W_3) (figure 12) is not part of the local unfolding of X_9 but part of $Y_{2,2}^1$. The condition for equal roots ξ^2 in (20) gives the lips locus as

$$W_3' = -\frac{3}{5\alpha} \kappa^2 = -\frac{1}{600} \kappa^2 \quad (\kappa \approx 0). \quad (21)$$

To obtain a better approximation to the lips locus far from $\kappa = 0$ requires higher order terms, as we shall see in §8.

Figure 12 shows a butterfly locus at $K = -3$ ($W_3 > 0$), the wings opening out

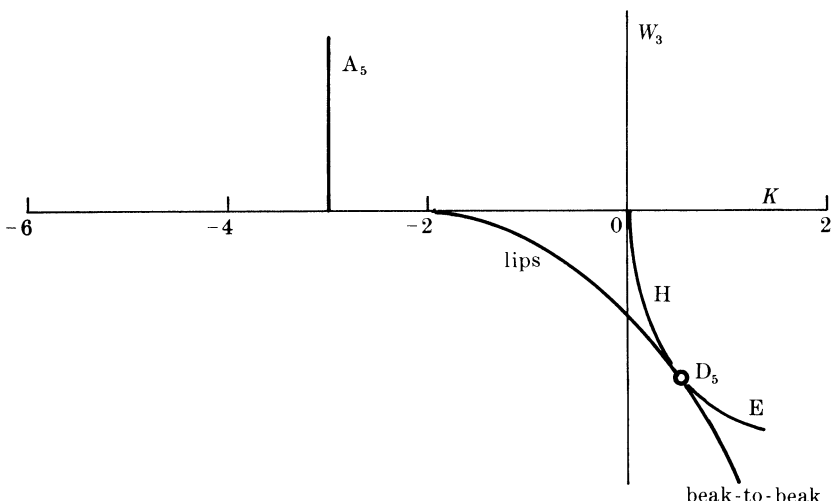


FIGURE 12. Loci in (K, W_3) space of the four butterflies (A_5), four parabolic umbilics (D_5), hyperbolic umbilics (H), elliptic umbilics (E), lips and beak-to-beaks.

on the side $K > -3$. This is part of X_9 and so may be calculated by retaining terms up to fourth order only in the expression (16) for ϕ . These results for lips and butterfly are consistent with the observations. However, diffraction causes ghostly prebrightening on the ‘wrong’ side of the lips locus, that is on the side where geometrical optics predicts no caustic. A similar effect is seen on the ‘wrong’ side (the cusp side) of the butterfly locus. The lips first manifest themselves (figure 3f) as elongated patches of light just outside each cusp.

6. THE UMBILIC LOCUS

So far our explanations of the observed caustics have needed no arbitrary parameters. This is because up to terms of order 6 in the wavefront the coefficients are all fixed, in terms of K , by the symmetry and the differential equation, rather than by the boundary condition (the square hole). More subtle features that involve terms of order 8 and higher in the wavefront do depend on the shape of the aperture. In fact in order 8 one parameter adjustable by the aperture shape enters, and in order 12 one more. We could, of course, solve the differential equation for the drop shape numerically and determine the higher coefficients, but our approach will rather be to infer the sign (which is what matters for the main features of the caustics) of the order 8 parameter from the observations.

Figure 12 shows the observed forms of the umbilic and lips loci. Starting at $K = 0$, $W_3 = 0$ and focusing downwards one at first sees the hyperbolic umbilic foci (H in figure 7r), but eventually these begin to unfold (figure 7s). However, by adding water very carefully, and so increasing K , one can prevent them unfolding on decrease of W_3 and so remain on the umbilic locus, as is done in figure 5. This shows that the locus curves in the sense shown in figure 12. We now explain this theoretically.

The condition for an umbilic point on the wavefront, whose height is $f(x, y)$, is

$$f_{xx} - f_{yy} = 0 \quad \text{and} \quad f_{xy} = 0 \quad (22)$$

and, if we use (10) and keep terms up to order 4, this gives

$$(6 - K)(x^2 - y^2) = 0 \quad \text{and} \quad Kxy = 0.$$

If $K = 0$, the second condition is satisfied and the first is satisfied for *all* points on $x = \pm y$. There is degeneracy; we have two *lines* of umbilics on the wavefront, rather than isolated points, and the pattern of lines of curvature is as in figure 13c. This explains why the four hyperbolic foci at first do not unfold as we focus downwards.

The fold condition $\phi_{xx}\phi_{yy} - \phi_{xy}^2 = 0$ together with $K = 0$ and $x = \pm y$, gives

$$(6x^2 + W_3)^2 = 0, \quad (23)$$

and so $W_3 < 0$. Thus, in the order 4 approximation the umbilic locus in the space (K, W_3) is the lower half of the line $K = 0$.

To resolve the degeneracy in the wavefront it is necessary to include terms up to order 8, satisfying the symmetry, thus

$$\begin{aligned} f = & \tfrac{1}{4}(x^2 + y^2) + C(x^4 + Kx^2y^2 + y^4) + C(Ax^6 + Bx^4y^2 + Bx^2y^4 + Ay^6) \\ & + C(Lx^8 + Mx^6y^2 + Nx^4y^4 + Mx^2y^6 + Ly^8) \quad (l = l_0). \end{aligned} \quad (24)$$

If symmetry is the only restriction, the new constants L, M, N may have any values. But, if we demand that they satisfy the differential equation (5), then (putting $l = l_0$)

$$M = \frac{1}{720}(12 - K) - 28L, \quad N = \frac{1}{144}(K - 6) + 70L. \quad (25)$$

Thus, apart from K (which fixes C, A, B), there is now just one arbitrary constant, namely L , to be fixed by the boundary condition.

The first umbilic condition in (22) continues to give $x = \pm y$, but the second now gives

$$x^2\{4K + \frac{2}{3}Kx^2 + 8(3M + 2N)x^4\} = 0. \quad (26)$$

When $K = 0$ the only root is $x = 0$ (sixfold). When $K \neq 0$, $x = 0$ continues to be a root (twofold), but the existence of other real roots depends on the sign of $3M + 2N$, which we shall show to be negative. The conclusion is that the other four roots of (26) are real provided $K > 0$. Thus the terms of order 8 in the wavefront cause the umbilic locus in (K, W_3) to curve away from $K = 0$ towards positive K , and this is in accord with observation (figure 12). Notice that order 6 terms (put $L = M = N = 0$) do not break the degeneracy.

To confirm the sign of $3M + 2N$ first note that, because of the orientation of the square aperture (with sides parallel to Ox and Oy), the coefficient c_8 in (8) is negative (c_4 is positive and $\cos 8\theta$ must reinforce $\cos 4\theta$ at $\theta = \frac{1}{4}\pi$) and correspondingly L is negative. Now, from (25),

$$3M + 2N = \frac{1}{720}(7K - 24) + 56L$$

and since $K \approx 0$ the expression is negative.

To find the equation of the umbilic locus we concentrate on the roots of (26) that depend on K ; x and K being small we find

$$x = \left\{ -\frac{K}{2(3M + 2N)} \right\}^{\frac{1}{4}} \quad (x, K \text{ small})$$

and then, from the mapping $x \mapsto W_3$ in (23), valid for K small,

$$W_3 = -6 \left\{ -\frac{K}{2(3M + 2N)} \right\}^{\frac{1}{2}}. \quad (27)$$

The observations in figures 5 and 12 show that although the umbilic locus leaving $K = 0$, $W_3 = 0$ is hyperbolic it encounters a parabolic umbilic point (D_5) and changes character to elliptic. To understand this we retain terms up to order 8 in the wavefront, evaluate third derivatives of f , put $x = y$, and use the elliptic-hyperbolic discriminant given by Berry & Hannay (1977). We note that it has the same sign as

$$-x^2\{36 + 18K + (6 + 7K)x^2 + 252(\frac{1}{240}(K - 2) + 16L)x^4\}.$$

Since $K > 0$ for the umbilic locus all terms within the braces are positive except possibly the coefficient of x^4 . As x increases the expression will eventually change sign from negative (hyperbolic) to positive (elliptic) if

$$\frac{1}{240}(K - 2) + 16L < 0.$$

We have seen that L is negative and so the condition is fulfilled. It follows that the four hyperbolic umbilic foci will eventually transform, first to parabolic

umbilics and then to elliptic umbilics, as water is added to the drop, or as the hole is made more circular. Occurring, as they do, on the main fold, the four D_5 singularities seem to be closely related to the two D_5 singularities that were observed (Nye 1979) as non-local features of E_6 and later interpreted by Callahan (1982b) as organized by X_9 ($K = -6$).

7. UMBILIC REACTIONS ON THE WAVEFRONT

It is easy to show that when $K = -6$ the lines of principal curvature on the wavefront are as in figure 13a, with singularity index -1 (this means that on a clockwise circuit around the origin the lines rotate by 2π anticlockwise), while for $K = +2$, which makes the wavefront circularly symmetric up to eighth order, they are as in figure 13e, with index $+1$. Non-degenerate umbilic points have indices $\pm \frac{1}{2}$. The change of sign of the central degenerate umbilic point takes place as K reaches zero and becomes positive (figure 13d), and, by symmetry, the arrangement of indices must be as shown. At $K = 0$ the central -1 umbilic emits four $-\frac{1}{2}$ umbilics and conserves total index by changing to $+1$. (Without the constraint of the differential equation the umbilic locus in (W_3, K) could curve the other way, and then the reaction could be on the negative K side, with four $+\frac{1}{2}$ umbilics coming in from infinity to change the central -1 to $+1$, figure 13b.)

The four outer umbilics are always hyperbolic when close to the origin. This is

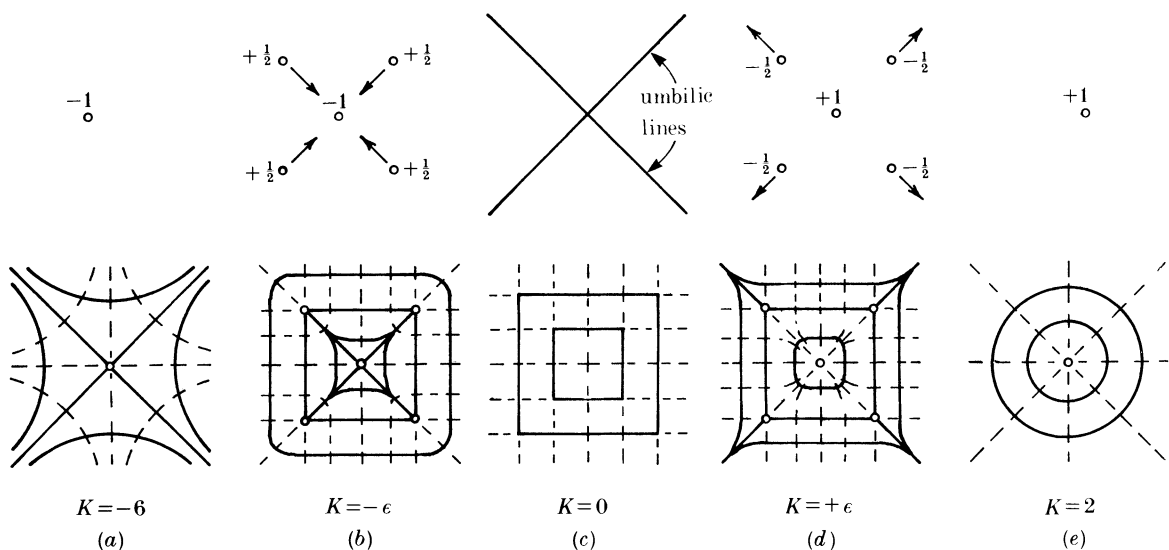


FIGURE 13. The five upper diagrams show how the umbilic points on the initial wavefront (and on the surface of the drop), and their singularity indices, behave as K increases from -6 to 2 . The five lower diagrams show the corresponding lines of curvature. As water is added to the drop the observed sequence is (a), (d), (e). Without the constraint of the differential equation the sequence could be (a), (b), (e). The four outer umbilics in (d) begin as hyperbolic stars but change to elliptic stars as water is added, being momentarily parabolic umbilic points. (c) shows the degenerate pattern associated with X_9 alone at $K = 0$; terms of order 8 are needed to break the degeneracy to (b) or (d).

because, for small x , and therefore small K , the hyperbolic or elliptic discriminant is unconditionally negative. In a similar way the line discriminant indicates that there are three straight curvature lines passing through each outer umbilic. The outer umbilics are therefore, in the Berry–Hannay nomenclature, hyperbolic stars (or, with no constraint from the differential equation and the umbilic locus curving the other way, hyperbolic monstars). Figure 13*b, d* shows how the terms of order 8 in the wavefront break the degeneracy of the umbilic lines seen in figure 13*c*. As they go through the parabolic transition the outer umbilics in figure 13*d* change from hyperbolic star to elliptic star.

The central umbilic point, with index ± 1 , remains degenerate throughout all these transitions. Its degeneracy can only be broken by perturbing the 4-fold symmetry, for example, by changing the aperture from a square to either a rectangle or a rhombus. Holes of these symmetries with thin drops ($-6 < K < -2$) give two elliptic umbilics of index $-\frac{1}{2}$ (Nye 1978); for thicker drops, in the range $-2 < K < 0$, the umbilics may be hyperbolic or elliptic depending on the perturbation (ϵxy or $\epsilon(x^2 - y^2)$), with index $-\frac{1}{2}$; for $K > 0$ they are hyperbolic with index $+\frac{1}{2}$. In fact, because the central umbilic point is structurally unstable, it is only too easy to break it up; the experimental difficulty is to preserve it.

8. THE LIPS LOCUS TO HIGHER ORDER

The parabolic umbilic (D_5) point in (K, W_3) will necessarily be the origin of a lips and beak-to-beak locus (figure 12) and of a swallowtail locus. In fact, the lips locus is the one we have already encountered emanating from $(K = -2, W_3 = 0)$ and organized by $Y_{2,2}^1$. This may be seen as follows. First note that the lips and parabolic umbilics all arise from points on the wavefront on the diagonals $x = \pm y$. We use the 45° axes with coordinates ξ, η . The condition for the lips on $\eta = 0$ is equal roots of $\phi'_{\xi\xi}(\xi) = 0$ (see figure 11): that is, $\phi'_{\xi\xi} = 0, \phi''_{\xi\xi\xi\xi} = 0$. As K increases from -2 the lips point on $\eta = 0$ on the wavefront changes, and for a particular K ($K > 0$) the lips condition and the umbilic condition can be satisfied simultaneously. This defines the D_5 point. If we retain only terms up to order 6 the lips locus from $K = -2, W_3 = 0$ never reaches the D_5 point, but goes to infinity on the asymptote $K = -\frac{6}{7}$. Including terms of order 8 and so obtaining a locus valid further from its origin makes it pass through the D_5 point.

At $K = 0, W_3 = 0$ the X_9 caustic consists (figure 8*b*) of two straight lines at right angles. These are, in fact, cusp lines that lie exactly in the plane of focus. Close observation shows that away from the centre of the field, $W_1 = W_2 = W_3 = 0$, they curve downwards very slightly towards negative W_3 , so that one is really (in figure 5*a*) observing two very elongated crossed lips. To explain this theoretically, terms of order 6 are not sufficient. Terms of order 8 are needed, and the sign of their coefficient L is indeed consistent with the observed direction of bending.

9. UNFOLDING FOR $0 < K < 2$

Figure 14 shows a focusing sequence with $0 < K < 2$ and crossing the elliptic umbilic locus. Moving upwards, the four cusps on the lowest figure first retract (*b–c*) to become four small curvilinear triangles (this is part of the parabolic umbilic

unfolding and involves first swallowtails and then ‘beak-to-beak’ (see, for example, figure 7 of Nye (1978))). These contract to points (*d*) as we cross the elliptic umbilic locus, and then expand again to become very large (*e* and *f*). The caustics in these patterns were much larger than the field of view of the microscope and could be viewed only one portion at a time (a lower power objective tends to cut out oblique rays and can lead to spurious observations). The beak-to-beak transition shown in figure 14(*f-g*) is hard to be sure of observationally because of unavoidable asymmetries and because of the extreme elongation of the pattern, but is very plausible. Thereafter the 8-cusped central figure and its surrounding oval contract without further change to a point at $W_3 = 0$. Meanwhile the outer figure has passed through four butterflies and the cusps then move to large angles.

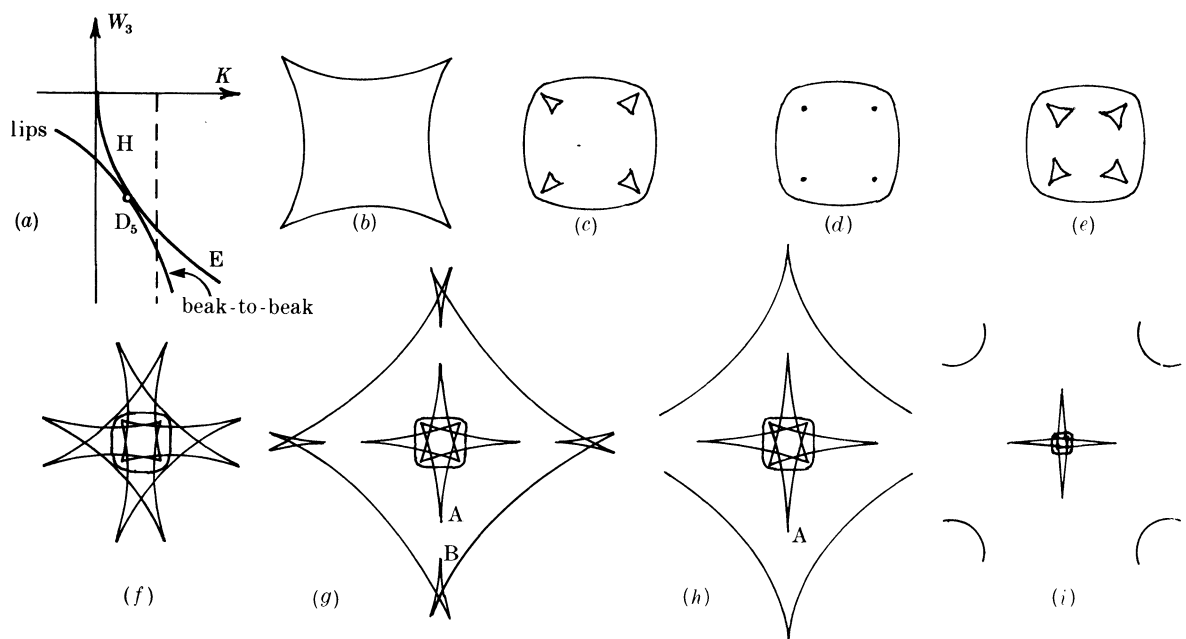


FIGURE 14. Sequence of observed caustics (not to scale) moving upwards along the broken line shown in (*a*), crossing the elliptic branch of the umbilic locus (diagram (*d*)). The beak-to-beak locus shown in (*a*) is the one that is associated with the events between (*b*) and (*c*), organized by the parabolic umbilic. There must be another beak-to-beak locus, not shown in (*a*), marking the transition between (*f*) and (*g*).

By including terms in the wavefront up to order 8 and examining the line $x = 0$ for cusps ($\phi_{xx} = 0$) we find no more than cusp A in the central figure in (*g*) and (*h*). However, by considering that at the edge of a square hole, on $x = 0$, $f_{xx} = 0$ we can show that another root of $\phi_{xx} = 0$ must be encountered, and this is the cusp B of the outer figure. The beak-to-beak event involving cusps A and B is thus inevitable.

10. PENDENT DROPS

Water drops made to hang downwards from the lower surface of the glass supporting-slide will have different shapes from the sessile drops considered so far, and one might expect a different range of caustics when they are illuminated. With the light incident from above or below there are four possible cases (figure 15), denoted su, sd, pu, pd (for 'sessile up', etc.).

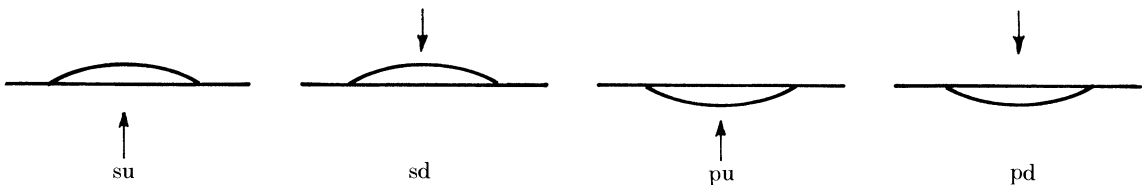


FIGURE 15. Drops above and below the supporting glass slide with the light, whose direction is shown by the arrows, incident from above and below. The four possible cases are shown (s, sessile; p, pendent; u, light direction up; d, light direction down).

Consider first pendent *thin* drops (cases pu and pd); the differential equation (5) for the wavefront now has a sign change, thus

$$\frac{\partial^2 f}{\partial x^2} + \frac{\partial^2 f}{\partial y^2} = 1 - \left(\frac{l}{l_0}\right)^2 f. \quad (28)$$

The solution up to sixth order is still given by (10) except that, with K in the range $-6 < K < 2$, the coefficient C of the fourth-order terms is now negative, and (11) is replaced by

$$K = -\frac{1}{8C} \left(\frac{l}{l_0}\right)^2 - 6.$$

The coefficients of the sixth-order terms retain their previous positive values. Since C does not appear in the potential ϕ given by (16) it does not affect the caustics of X_9 referred to controls W_1, W_2, W_3 ; but it does enter the scalings (15) and, in particular, it reverses the sense of W_3 relative to Z (Z is measured in the direction of the light). We expect the X_9 caustics to be inverted through the focus, relative to the direction of light, and turned through 45° . Figure 7 shows that these operations leave the caustics unchanged in general form when $-6 < K < -3$, but for $K > -2$ the change is drastic. For example, with a circular hole ($K = 2$) a sessile drop on top of the slide (cases su and sd) should give a spun cusp pointing away from the drop, with an axial caustic line (figure 16a); whereas a pendent drop (cases pu and pd) should give a spun cusp (and axial line) pointing towards the drop (figure 16b). The relative signs of the fourth- and sixth-order terms mean that for a pendent drop the modulus in $Y_{2,2}^1$ becomes $+1$, in place of -1 .

When these theoretical expectations were tested by observation they were at first thought to be wrong; some of the pendent drops gave confusing caustic patterns and others gave the standard caustic sequences associated with sessile drops. The experiments were also more difficult. Hanging drops cannot be made

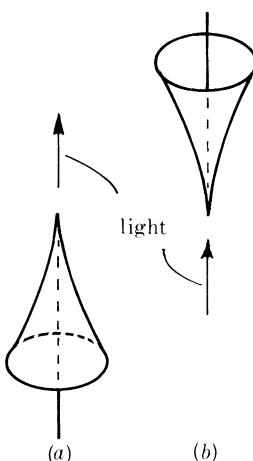


FIGURE 16. The spun cusp with its axial caustic line pointing (a) away from the drop and (b) towards the drop.

in holes larger than a critical size, because they fall off. For a long slit of width w one may show (Nye *et al.* 1984, figure 5) that, if $w > 2\pi l_0$, no solutions for the drop profile exist that satisfy the boundary conditions and that also keep the drop thickness everywhere positive. The key to the paradoxical caustics was found by observing a drop hanging from a slightly elliptical hole of mean diameter 10.7 mm (i.e. $4l_0$). An inverted microscope was used with the light incident from above (case pd). With very little water the slightly perturbed spun cusp pointed towards the drop, as predicted, but with more water added it reversed in direction and pointed away from the drop. In other words, the spherical aberration reversed in sign. Evidently, with drops having large slopes the non-paraxial effects always combine to produce the ‘standard’ caustic sequences of figure 8*b*, with the perturbed spun cusp pointing away from the drop. This is so whichever way up the drop is. For sessile drops gravity reinforces the non-paraxial effects, and so the combined result is always the standard sequence. However, for pendent drops the effect of gravity, which tends to make the spun cusp point towards the drop, opposes that of non-paraxiality; there is then a competition, which has the result of reversing the spun cusp as the drop becomes thicker.

With a thin drop it makes no difference to the caustics whether the illumination is from above or below, as would be expected. Thin pendent drops in square holes give X_9 patterns inverted through the focus and turned through 45° , as paraxial theory predicts (in fact, when the side a of the square is less than 6 mm, $-6 < K < -3$ so that the inversion is not apparent, but when $a \geq 7$ mm, $-2 < K < 2$ and the inversion is clear).

However, the direction of the light does make a difference when the pendent drop is thick, because the non-paraxial effects are different: in case pd all the refraction takes place at the curved surface, while in case pu it is spread between both surfaces of the drop, and so spherical aberration arising from nonlinearity in Snell’s law is reduced. This is clearly shown in observations of pendent thick drops in square holes. Pendent drops loaded until they are about to fall off always give standard

(non-inverted) X_9 patterns when illuminated from above (case pd), whatever their size. This is because of the overwhelming non-paraxial effects. However, the same drops illuminated from below (case pu) show an interesting changeover when the side a of the square is close to 7.3 mm (i.e. $2.7l_0$). This value of a gives standard X_9 patterns with $K \approx 0$ (figure 18, plate 9), while a slightly larger value gives inverted X_9 patterns with $K \approx -1$. The transition is subtle, with a change in a of 0.1 mm making a significant difference. The same transition in the same direction can also be brought about with a fixed at 7.3 mm by thinning the drop and so increasing the focal length $2R_0$ from 6 to 30 mm (compare figure 18 with figure 20).

To explain this effect we introduce coefficients $p = C$, $q = \frac{1}{2}CK$ and write the wavefront as

$$f = \frac{1}{4}(x^2 + y^2) + px^4 + 2qx^2y^2 + py^4 + O(6),$$

noting that it is no longer necessarily subject to the constraint of the differential equation (28), and we consider the parameter space p, q (figure 17). The value of

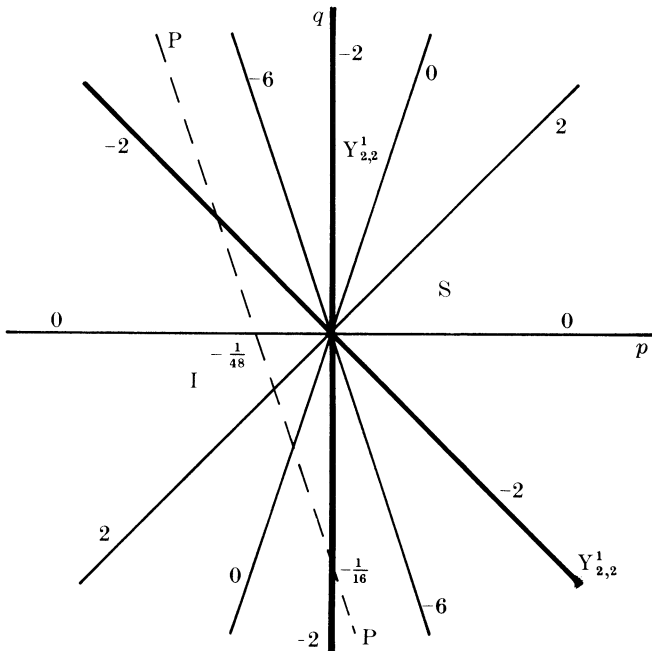


FIGURE 17. The space of coefficients p, q defining the fourth-order terms. Values of K are shown on the radial lines. The X_9 caustic patterns are standard (S) to the right of $K = -6$, but inverted through the focus and turned by 45° (I) to the left of $K = -6$. For thin pendent drops the coefficients lie on the locus PP (taking $l = l_0$).

K in the range $-6 < K < 2$ is shown by the radial lines. Changing a and the thickness of the drop corresponds to changing p and q . The X_9 caustics invert and turn through 45° across the line $K = -6$. For thin pendent drops the locus in p, q space is the line PP. The line $K = -2$ corresponds, as we have seen, to the singularity $Y_{2,2}^1$. By appropriate choice of the side a and the drop thickness it is

possible to make both p and q zero. Experimentally this is evidently close to $a = 7.3$ mm and with the thickness near to its maximum achievable value. Then K will be indeterminate and it will not be possible to say whether the X_9 pattern is standard or inverted. The germ of the singularity will now be

$$x^6 + rx^4y^2 + rx^2y^4 + y^6.$$

Because the term in x^2y^2 has disappeared the singularity is no longer $Y_{2,2}^1$; in fact it is not a member of any family in Arnold's (1975) list.

At this critical transition the slightest deviation from symmetry produces distinctive new caustic patterns (figure 19a–g, plates 10 and 11) in which two parabolic umbilics 'nose-to-nose' are prominent, recognizable from their characteristic diffraction patterns. The levelling of the microscope, the adjustment of the direction of illumination and the suppression of vibration all become important if one is to obtain fourfold symmetric caustics. A focusing sequence near the transition and corresponding to $-6 < K < -3$ is shown in figure 20. As the plane of focus is lowered note how the four non- X_9 folds (shown broken) come in and make beak-to-beak interactions, which are followed by four butterfly singularities, to leave at the lowest level four inward-pointing cusps (figure 20g and 19h). As far as the start and finish are concerned, this is the same as the sequence of patterns for $K \approx -1$ in figure 7, but inverted and turned through 45° . These beak-to-beak events produced by the extra folds are analogous to the lips events produced by the extra folds in the standard sequences of figure 7.

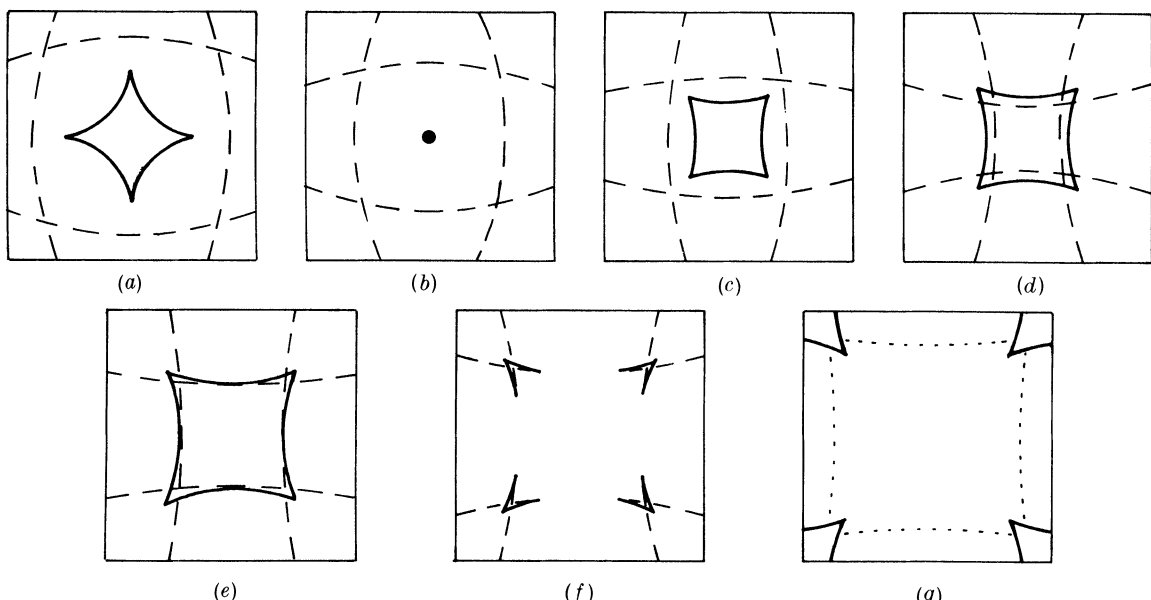


FIGURE 20. Sketches of the caustics (not to scale) from a water drop hanging from the lower surface of a slide and illuminated from below. The hole was a square of side 7.3 mm and it was filled to give a focal length $2R_0 = 23$ mm. Parts (a)–(g) show a focusing sequence moving downwards towards the drop. The dotted line in (g) is not a caustic but denotes strong diffracted intensity. The inner figure in (a)–(c) indicates a standard X_9 sequence with $-6 < K < -3$. However, the four inward-pointing cusps in (g) indicate $K \approx -1$ and a sequence inverted and turned through 45° .

11. WATER DROPS OF OTHER SYMMETRY AND OF NO SYMMETRY

11.1. *The transition from elliptic to hyperbolic umbilic points*

We return now to sessile drops, but we relax the fourfold symmetry imposed up to this point. The shape of sufficiently small and sufficiently thin water drops of all outlines is governed by Poisson's equation, and this also governs the shape of the wavefront emerging from the drop. All umbilic points are then of elliptic type and they essentially organize the caustic pattern (Nye 1978). As a drop is made larger or more highly curved the wavefront ceases to obey Poisson's equation and hyperbolic umbilic points become possible. The first indication of new caustic structure is the appearance of lips near the outward-pointing cusps. These then provide the extra folds that are necessary for the hyperbolic umbilic foci. We have seen that for 4mm symmetry the lips themselves are *not* explained by X_9 , although X_9 does explain the outer fold of the lips; one needs $Y_{2,2}^1$, which appears at a value of the X_9 modulus that is forbidden to X_9 itself, namely $K = -2$.

The change from elliptic to hyperbolic umbilic points as a drop is made larger may be understood by considering a thin, small drop spanning an aperture that has the symmetry of a regular polygon of n sides ($n > 2$). The corresponding wavefront has the form

$$f = \frac{1}{4}r^2 + a_n r^n \cos n\theta + a_{2n} r^{2n} \cos 2n\theta + \dots$$

At the centre there is an umbilic point with index $\frac{1}{2}(2-n)$, which may be regarded as the superposition of $n-2$ elliptic umbilic points each of index $-\frac{1}{2}$. If water were added to this drop to make it more bulbous, it would (if it did not transgress its perimeter) ultimately approach an oblate spheroid of revolution. The wavefront would also be an oblate spheroid, and therefore would have at its centre an umbilic point of index +1. This may be regarded as the superposition of two hyperbolic umbilic points, each of index $+\frac{1}{2}$ (which would separate if a small perturbation were applied). Generalizing from the case $n = 4$, we may presume that the transition from index $\frac{1}{2}(2-n)$ to index +1 is made by n umbilic points of index $-\frac{1}{2}$ leaving the centre (or, less likely, n umbilic points of index $+\frac{1}{2}$ entering the centre from the sides). Notice that a circular aperture ($n \rightarrow \infty$) spanned by a thin, small drop gives part of a sphere, which is umbilic *everywhere*; an n -fold symmetric perturbation ($n > 2$) leaves the centre as an isolated, although degenerate, umbilic point. However, with a large drop affected by gravity the central umbilic is already an isolated point and it remains so under an n -fold symmetric perturbation.

11.2. *Caustic patterns*

At $K = 2$ the terms of order 4 in the wavefront (10) become isotropic, and the coefficient c_4 in (8) and (9) becomes zero. Anisotropy is now provided by terms of order 8 and higher; it is these that break the degeneracy of X_9 at $K = 2$ shown in figure 10a by the intersection of the two coincident circles. By adding water to a drop in a square hole we never reach the limit $K = 2$, but it is approached quite closely (for example, in figure 6d). Making the aperture approach a circle, but keeping 4mm symmetry, would make the central caustic in figures 6d and 7x

approach an ever-smaller regular 8-cusped star. At the limit itself we can recall that the degenerate three-dimensional caustic given by a perfectly circular hole is the spun cusp (figure 16) with a caustic line along the negative W_3 axis. This is highly unstable. A small perturbation with 4mm symmetry changes the spun cusp only slightly, so that its section is a fourfold symmetric oval, but the axial line is radically broken up so that its section unfolds from an isolated point to an eight-cusped star.

The X_9 caustics associated with 2mm symmetry (which can be readily produced from water drops in rectangular or rhombus-shaped apertures) are abundantly illustrated by Upstill (1979). Those corresponding to $K = 2$ result from breaking the perfect circular symmetry of the spun cusp to give the focusing sequence of figure 21a–e. These patterns, one of which is photographed in figure 6g, occur in many different physical contexts. They include: the centro-surface of an ellipsoid, analysed by Cayley (1873); the primary (Seidel) aberrations of a lens system (Berry & Upstill 1980, Appendix 2); astigmatism of electron lenses (Leisegang 1953); the occultation of a star by the planet Mars with the Martian atmosphere acting as a lens with broken circular symmetry (Elliot *et al.* 1977; Berry 1981); the passage of seismic waves through the not-quite-spherical Earth to ‘focus’ on the opposite side of the globe (Nye 1985); rainbow formation by spheroidal water drops (Nye 1984). A more complex pattern with 2mm symmetry, but not organized by X_9 , has already been noted in figure 19a–g.

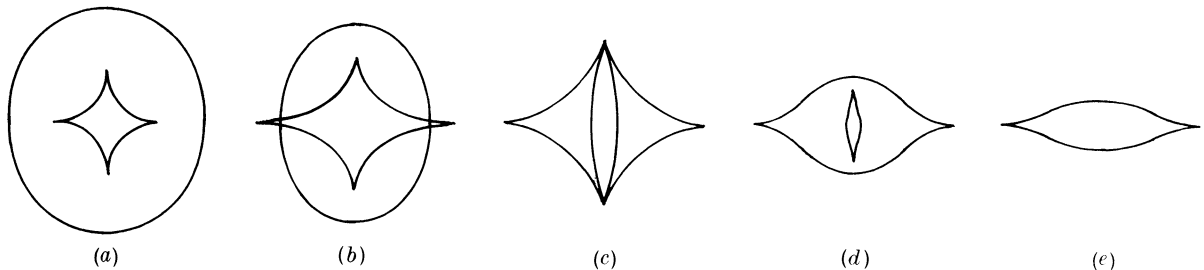


FIGURE 21. Focusing sequence for symmetry 2mm, showing two hyperbolic umbilics at (c), and lips events between (d) and (e) and beyond (e). Pattern (b) is seen in figure 6g.

If the symmetry were 3m (equilateral triangle) the addition of order 4 terms that preserve the symmetry is only possible if they are isotropic, that is $K = 2$. This results in the ‘compactified elliptic umbilic’, illustrated by Upstill (1979), and seen, with some asymmetry, in figure 6e. Its caustic patterns are also shown by Lenz (1956) in connection with experiments in an electron microscope made by altering the lens controls. For symmetry 5mm (pentagon), 6mm (hexagon), etc., once again, order 4 terms would break the symmetry unless $K = 2$. Thus the twofold and fourfold symmetries are the only ones that allow X_9 , with its full range of K , to participate, and this is why fourfold symmetry was chosen for the present study.

The eight-cusped star pattern for 4mm symmetry is typical of the caustic pattern found near the focus for the higher symmetries: an oval containing a multi-cusped figure. The general result is that the symmetry of a regular n -gon ($n > 2$) produces

an oval and a figure having two sets of n cusps, arranged on two circles, making $2n$ cusps in all.

We conclude with a few examples of how the inner cusped figure changes as one passes from one symmetry to another. Figure 6g compared with (h) and (i) shows how the symmetry can be broken from 2mm to m, with the appearance of a butterfly at the bottom of figure 6h. In figure 6i, which is from the same drop further from the focus, two unfolded butterflies, with 8 cusps in all, have produced a caustic that is close to figure 6d. In this way butterfly singularities provide the extra pairs of cusps needed in the transition from lower to higher symmetry. Swallowtail singularities may also participate, as exemplified by the one seen, slightly unfolded, in the centre of figure 6f, which is from a highly curved, but unsymmetrical, water drop. As figures 6d–i all illustrate, the oval is ubiquitous and very stable; it comes from the radial curvature of the drop. The cusped figure, on the other hand, comes from the circumferential curvature and is highly sensitive to the details of the shape. The glint of the Sun reflected in a dewdrop, and seen by the naked eye as a bright point, must possess a similar microscopic caustic structure.

I thank Dr C. Upstill and Dr J. V. Hajnal for suggesting several improvements in presentation, which have been incorporated in the paper.

REFERENCES

- Arnold, V. I. 1975 *Russ. math. Surv.* **30**(5), 1–75 (transl. of *Usp. mat. Nauk* **30**(5), 3–65).
 Berry, M. V. 1976 *Adv. Phys.* **25**, 1–26.
 Berry, M. V. 1981 In *Physics of Defects, Les Houches, Session 35, 28 July–29 August 1980* (ed. R. Balian, M. Kléman & J. P. Poirier) (Amsterdam: North Holland), pp. 453–543.
 Berry, M. V. & Hannay, J. H. 1977 *J. Phys. A* **10**, 1809–1821.
 Berry, M. V. & Upstill, C. 1980 *Prog. Optics* **18**, 258–346.
 Callahan, J. 1982a *Proc. Lond. math. Soc.* **45**, 227–257.
 Callahan, J. 1982b *Proc. R. Soc. Lond. A* **382**, 319–334.
 Cayley, A. 1873 *Trans. Camb. phil. Soc.* **12**, 319–365. (Also in *Collected mathematical papers*, vol. 8, no. 520, 316–365 (1895). Cambridge University Press.)
 Elliot, J. L., French, R. G., Dunham, E., Giersch, P. J., Veverska, J., Church, C. & Sagan, C. 1977 *Astrophys. J.* **217**, 661–679.
 Hajnal, J. V., Templer, R. H. & Upstill, C. 1984 *Eur. J. Phys.* **5**, 81–87.
 Leisegang, S. 1953 *Optik* **10**, 5–14.
 Lenz, F. 1956 In *Proc. 3rd Int. Conf. on electron microscopy, London 1954*, pp. 83–85. London: Royal Microscopical Society.
 Nye, J. F. 1978 *Proc. R. Soc. Lond. A* **361**, 21–41.
 Nye, J. F. 1979 *Phil. Trans. R. Soc. Lond. A* **292**, 25–44.
 Nye, J. F. 1984 *Nature* **312**, 531–532.
 Nye, J. F. 1985 *Geophys. Jl R. astr. Soc.* **83**, 477–486.
 Nye, J. F., Lean, H. W. & Wright, A. N. 1984 *Eur. J. Phys.* **5**, 73–80.
 Upstill, C. 1979 Catastrophe optics and caustic networks. Ph.D. thesis, University of Bristol.
 Upstill, C., Wright, F. J., Hajnal, J. V. & Templer, R. H. 1982 *Optica Acta* **29**, 1651–1676.